5-2013

AN EXPERIMENTAL STUDY OF SUPERSONIC CAVITY FLOW CONTROL WITH VERTICAL RODS

Carolyn Leigh Thiemann
cthieman@utsi.edu

To the Graduate Council:

I am submitting herewith a thesis written by Carolyn Leigh Thiemann entitled "AN EXPERIMENTAL STUDY OF SUPERSONIC CAVITY FLOW CONTROL WITH VERTICAL RODS." I have examined the final electronic copy of this thesis for form and content and recommend that it be accepted in partial fulfillment of the requirements for the degree of Master of Science, with a major in Aerospace Engineering.

Ahmad D. Vakili, Major Professor

We have read this thesis and recommend its acceptance:

Trevor M. Moeller, U. Peter Solies

Accepted for the Council:
Carolyn R. Hodges

Vice Provost and Dean of the Graduate School

(Original signatures are on file with official student records.)

AN
EXPERIMENTAL STUDY OF SUPERSONIC CAVITY FLOW CONTROL WITH VERTICAL RODS

A Thesis

Presented for the

Master of Science

Degree

The University of Tennessee, Knoxville

Carolyn Leigh Thiemann

May 2013

ACKNOWLEDGEMENTS

I would like to thank everyone involved in helping work on this thesis as well as this school and its staff which provided me with such a great opportunity to further my education. Thank you to my advisor, Dr. Ahmad Vakili, for his guidance and insight as well as the opportunity to work on this amazing project.

Thank you to Dr. Trevor Moeller and Dr. U. Peter Solies for agreeing to take the time to be on my committee, as well as offering their knowledge and guidance in its completion.

Also, I'd like to thank Garrett Milne, without whom I would not have had a basis for building my work.

I wish to give a particular thanks to the Gas Dynamics Lab personal, Joel Davenport, Chris Armstrong, Andrew Davis and Jack LeGeune, who spent countless hours running the wind tunnel, fixing problems and helping me change configurations. I owe them more than I can say, and I appreciate their contribution greatly.

Finally, I'd like to say a big thank you to all my friends and family who have encouraged and helped me as I worked towards completing this thesis. They helped me get through the long days and endless nights and come out a better person.

ABSTRACT

Analysis of an open cavity shear layer when exposed to different leading edge pin configurations was studied experimentally, in a blow-down high speed wind tunnel run at Mach 1.84. A non-intrusive quantitative flow measurement system, Particle Image Velocimetry, was used to study velocity and vorticity fields with and without flow control implementations. The purpose of this study was to attempt to understand and explain the flow mechanisms which cause acoustic suppression obtained using different leading edge, vertical pin configurations. The cavity had an L/D of 4.89 and each pin configuration had a varied number and placement of pins, while pin height remained a constant ½ inch. The four configurations chosen to be studied were based on the best acoustic suppression results obtained by Milne [4]. To determine and understand the physical mechanism and source of attenuation of this type of cavity flow control technique, this study looked at the acoustic spectrum, velocity vector field data as well as the changes in the velocity and vorticity fields created by each pin configuration. It was determined that a redistribution of the velocity and diffusion of the vorticity in the boundary layer was caused by altering the characteristics of the boundary layer. Vertical pin configurations at the leading edge of a cavity resulted in flow characteristics which bring about a thickening of the shear layer which diffuses the boundary layer vorticity. Certain pin configurations result in various changes in the boundary layer velocity and vorticity redistributions, affecting the shear layer diffusing the boundary layer vorticity. Configurations using staggered pin patterns generated more effectively vorticity diffusion in the shear layer, which lowered the peaks and the broadband in the SPL spectrum. Possible configurations for future testing are also recommended to further study the flow suppression mechanisms.

TABLE OF CONTENTS

LIST OF TABLES

LIST OF FIGURES

NOMENCLATURE

PIV	Particle Image Velocimetry
L	Length of cavity
W	Width of cavity
D	Depth of cavity
L/D	Cavity length to depth ratio
f	Frequency
U	Velocity magnitude
u	Velocity, x-component
v	Velocity, y-component
M	Mach number
K_v	Ratio of convective velocity of vortices to freestream velocity
m	Mode number for cavity oscillations
n	Phase delay between acoustic wave and new vortex
St	Strouhal number
γ	Specific heat ratio
θ	Momentum thickness
θ/L	Shear layer momentum thickness to length ratio
SPL	Sound Pressure Level
P	pressure

ω	Vorticity
dx	Particle displacement
dT	Time interval between two sequential images
a	local speed of sound
δ	boundary layer thickness
Re	Reynolds number

Subscripts

∞	freestream
o	stagnation

CHAPTER 1: INTRODUCTION

1.1 Background

In many different engineering problems and applications, enclosed openings or cavities will exist over which any encountering flows must span. The study of such situations is referred to as cavity flow, and it has many applications, such as in weapons bays, landing gear compartments and even in cars and tractor trailers. It is an important problem to study due to the possibility of undesirable flow patterns, increased drag, and large, potentially damaging pressure fluctuations which can be encountered under certain circumstances. An example of this is when a window is opened in a moving car, creating large amounts of noise and buffeting. While possibly distracting or uncomfortable for the occupants of a car which travels at a relatively slow speed, these effects could be potentially harmful at much higher velocities, such as on an aircraft. Here the results would be much more disastrous as addressed by Heller and Bliss [1] who pointed out the damage or stress that pressure fluctuations could cause on sensitive instruments or even the surrounding structure. A more in-depth review of the development of the study of cavity flow can be found in Chapter 2 of this thesis.

Cavity flow control is the use of various methods and techniques to help solve these difficulties by altering the flow field to avoid any potentially harmful effects. Many different techniques have been designed and used to do this, but the successfulness of each ultimately depended on the physical characteristics of the cavity and the flow interacting with it, as described by Rockwell and Naudascher [2] and later Plentovich, Stallings and Tracy [3]. For this reason cavity flow control has split into two separate branches of study, passive and active, each with their own strengths and weaknesses. Active flow control is defined by the fact that it provides an external energy to the flow while passive only works to alter the flow's existing energy. Passive control techniques such as ramps and fences have long been used due to their ease of implementation, despite the superior results of many active control techniques such as upstream mass-injection. This study looks into a new control method that, while passive, would be able to emulate the effectiveness of active control.

1.2 Objective

This study was focused on using a non-intrusive visualization method, Particle Image Velocimetry, to examine shear layer activity resulting from cavity flow control, based on the work of Milne [4]. Milne's research focused on measuring the suppression obtained using a unique passive control technique in supersonic cavity flow and many different configurations were tested as depicted in Table 1. The current study was concerned with taking a detailed look at only the most promising configurations, as determined through dynamic pressure readings by Milne. Therefore the objectives of this thesis include:

- To use Particle Image Velocimetry (PIV) to examine the velocity and vorticity fields in the cavity shear layer. This objective is for the purpose of determining trends in the most promising pin plate configurations and trying to determine why they were more successful.
- To determine further pin configurations for testing based on the determined success of the above objective.

Table 1- Pin Configuration key. (from Milne [4])

Run Name and Number	Description	Configuration
Key	Empty Hole, 1/8" pin, 1/4" pin, 3/8" pin, 1/2" pin	FLOW
1 – Baseline	Blank plate, no holes, no pins	
2 – Pin Plate Baseline	Pin plate with no pins	
3 – Full Plate, ⅛"	Pin plate full of ⅛" pins	
4A/B – Two rows, ½"	Two full rows of pins located at front (or rear) of pin plate	

Table 1 (continued)

Run Name and Number	Description	Configuration
Key	Empty Hole; 1/8 " pin; 1/4 " pin; 3/8 " pin; 1/2 " pin	FLOW
5 – Steady Ramp Wedge	Two full rows of ½" pins at edge of cavity, followed by one full row of ⅜" pins and decreasing by 2 pins per row and height. Two rows for each pin height	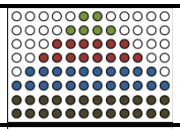
6 - Alt pin-hole, row-row	Alternating rows of pin-hole ½" pins followed by a row of no pins	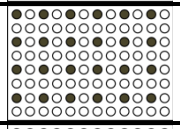
7 – Full Height Wedge	Wedge formed with ½" pins. Three full rows at edge of cavity, decreasing by two pins per row towards free stream	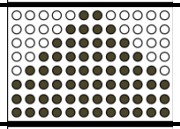
8A/B - Half Staggered, ½"	Staggered offset rows filling only 4 rows either at front or rear of plate, all ½" pins	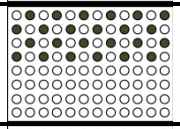
9A/B – Four rows, ½"	Four full rows of ½" pins located in the four rows nearest the cavity or at front of plate	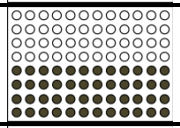
10 - Staggered ⅜"	Rows of alternating ⅜" pin-hole offset such that second row pin is behind first row hole	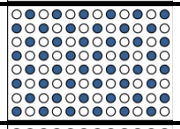
11 - Full Plate, ⅜"	All holes full of ⅜" pins	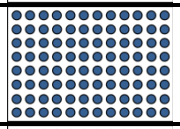
12 - Staggered Every 2nd Row, ½" **(Used in current study)**	Every 2nd row contains half the number of pins alternating pin-hole, next row is empty, and the following row hole is offset. ½" pins	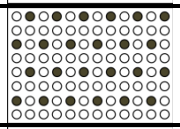
13 – Full Plate, ½" **(Used in current study)**	Pin plate full of ½" pins	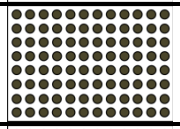
14 – Steady Ramp	Pins start at ⅛" and increase in height towards the cavity in two row increments	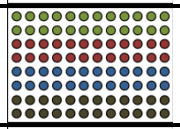
15 - Every other row open **(Used in current study)**	Alternating rows of ½" pins followed by a row of no pins	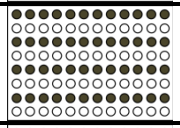
16 - Staggered Row-to-Row, ½" **(Used in current study)**	Each row contains half the number of pins alternating pin-hole, next row hole is offset. ½" pins	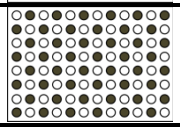

1.3 General Approach

Testing for this study took place in The University of Tennessee Space Institute (UTSI) Gas Dynamics Laboratory. A blow-down high speed wind tunnel (HSWT) was used in conjunction with a TSI LASERPULSE Particle Image Velocimetry system to determine velocity and vorticity fields. The wind tunnel has a converging/diverging nozzle designed to operate with the Mach number of 1.85 in the test section but actually functions best at Mach 1.84. The test section itself is an 8 inch by 8 inch square duct that is 4 feet long, with viewing panels of on either side and on top to allow for imaging within the test section. A full description of the wind tunnel setup and all other experimental layout and equipment are outlined in Chapter 3.

The cavity size used for this study was a length *L* of 11 inches, width *W* of 3 inches and depth *D* of 2.25 inches which results in an *L*/*D* of 4.89. This study looks at the effects of resonance in an open cavity, and this cavity's dimensions fall within this range, *L*/*D* less than 10. The removable plate at the leading edge of the cavity which housed the pin configurations was 3 inches wide to span the entire cavity and 2 inches in length. The dimensions for the cavity and pin plate are depicted in Figure 1.

Only the most promising pin configurations were chosen to be studied in this work. All of the configurations examined in the previous research by Milne [4] can be seen in Table 1, as well as the select configurations examined in this study. For the purpose of this study the following configurations were chosen to be further studied:

- Configuration 1- Baseline: This configuration was completely flat to simulate an unaltered leading edge surface. This was a necessary baseline with which to compare all results.
- Configuration 12- Staggered Every 2nd Row, ½ inch: This configuration had the least number of pins and the smallest decrease in the sound pressure level (SPL) at the dominant frequency.

- Configuration 13- Full plate, ½ inch: This configuration had the most number of pins and represents the second smallest decrease in SPL at the dominant frequency.
- Configuration 15- Every other row open, ½ inch: This configuration was the second largest decrease in SPL at the dominant frequency.
- Configuration 16- Staggered Row-to-Row, ½ inch: This configuration resulted in the largest decrease in SPL at the dominant frequency.

Further details on the selection of these configurations are provided in Chapter 3.

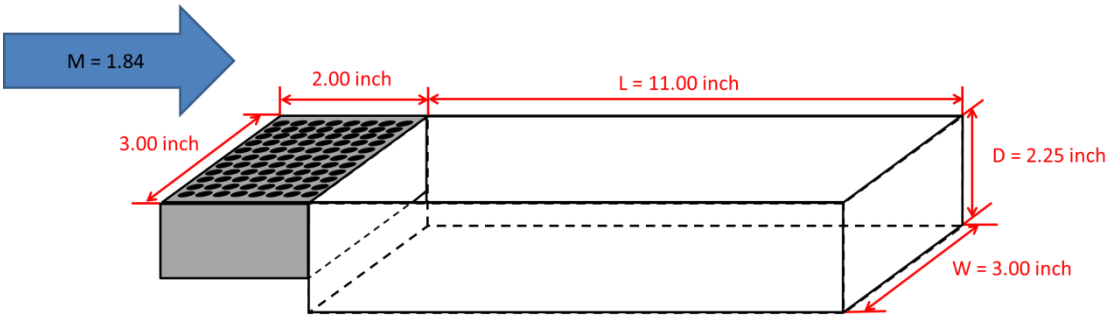

Figure 1- Cavity dimensions. (from Milne [4])

CHAPTER 2- TECHNICAL REVIEW AND ANALYSIS

2.1 Introduction

This chapter will cover a brief review of the history of cavity flow research from its start in the 1950s to its current state. This will be accomplished by looking at the fundamentals of cavity flow discovered as the field developed as well as a looking at some of the most important steps taken towards cavity flow control over the years. While this chapter is not capable of containing the extent of a complete and comprehensive review, the contents are sufficiently thorough to put this current study in perspective.

2.2 Cavity Flow Review

Studies focused on learning about cavity flow and understanding its effect began in the 1950s, due to a desire to find a solution to the harmful effects brought about by flow over a cavity. To do this they first had to understand what was going on inside the cavity, and therefore it was in these first few decades that some of the most fundamental and foundational research of this topic occurred. In 1955, Karamcheti [5] was studying the acoustic radiation due to varying lengths of shallow wall gaps in both subsonic and supersonic flow. Using Schlieren for his flow visualization and then optical interferometry and hot-wire anemometers for intensity and frequency measurements, Karamcheti's results showed some very fundamental concepts of cavity flow. One was that the frequency of a cavity's flow is inversely proportional to the cavity length for a fixed Mach number, for both a laminar and turbulent flow. Another was that the intensity of the acoustic field grew with increased speed, with Karamcheti measuring intensity as high as 160 decibels (dB) at Mach 0.8.

At the same time Roshko [6] was performing similar experiments with a cavity of varying length to depth ratio, but instead he was focused on the increase in drag due to the presence of a cavity. He concluded that, contrary to what had been supposed, friction contributions from the cavity were relatively negligible and were almost entirely from the pressures on the cavity walls. Roshko also made observations on the formation of vortices in the cavity and noted the very

important fact that high pressures at the trailing edge are due to the shear layer partially deflecting off this point and forming a vortex.

Study continued in this field but it wasn't until almost a decade later that the next great step forward occurred in the work of Rossiter [7]. Studying the unsteady pressures acting in and around a cavity, Rossiter came to the conclusion that while both random and period components were present, depending on the cavity L/D ratio one or the other component would dominate. For a shallow cavity ($L/D > 4$) the predominant component was random while for a deeper cavity ($L/D < 4$) it was more periodic. Rossiter also made note that there always seemed to be a dominant frequency which 'jumps' as the speed changes, as well as a set of secondary frequencies which he said seem to 'lie on a family of curves'. This is the basis for the empirical equation (1) which Rossiter is best known for developing. It calculates the cavity frequency based on flow parameters and empirically determined constants, as well as some as the then fairly new parameter m which Rossiter called the 'stage' number (now known as the mode number for cavity oscillations).

$$f = \frac{U_\infty}{L} \frac{(m-n)}{\left(\frac{1}{K_v} + M\right)} \qquad (1)$$

In this equation L represents the cavity length while U_∞ and M are the freestream velocity and Mach number respectively. For the two empirical constants, K_v is the ratio of convective velocity of vortices to freestream velocity, while n is the phase delay between acoustic wave and new vortex and will vary depending on L/D. Rossiter derived the values of these constants as K_v=0.57 and n = 0.25 for a L/D = 4.

This equation was later improved upon when Heller, Holmes, and Covert [8] found that for Mach numbers 0.8 and 1.5 Rossiter's equation worked very well, but for higher Mach numbers like 2 and 3, the difference between actual and predicted became larger and larger. They proposed that this was because when Rossiter developed his equation he took the cavity speed of sound to be the same as the freestream speed of sound (a cavity recovery factor of 0). For the lower Mach numbers tested by Rossiter this assumption created little error but as the Mach

number increased so did the error. To remedy this, a change was made to form the modified Rossiter's equation (2) where the speed of sound was assumed to be equal to the freestream stagnation speed of sound.

$$St = \frac{fL}{U_\infty} = \frac{(m-n)}{\left\{ \frac{M}{\left[1+\frac{(\gamma-1)}{2}M^2\right]^{1/2}} + \frac{1}{K_v} \right\}} \qquad (2)$$

In forming this modified equation the ratio of specific heats γ was introduced, as well as the non-dimensionalized cavity frequency, what we know as the Strouhal number *St*. The experimental results obtained by Heller, et al. proved that the updated equation could correctly predict the possible frequencies for a much larger range of Mach number than previously, but this still left the question of how to know which of these frequencies would actually be present in a cavity, and at what amplitude. This final question was left unanswered by Heller, et al. and has yet to find a satisfactory solution to this day.

In 1975, Heller and Bliss [1] worked to provide a more actuate description of the physical mechanism controlling cavity pressure fluctuations for the purpose of finding practical ways to suppress these oscillations. Using water table visualization techniques they realized that mass addition and withdrawal was occurring at the trailing edge due to the shear layer interacting with the cavity's internal fluid. This formed the basis for a cavity flow model in which the cavity's rear wall was replaced by an oscillating 'pseudo-piston'. This piston would generate forward traveling waves which would then reflect off the leading edge and become rearward traveling wave. They posited that this continued circulation effect creates an unsteady shear layer and results in the witnessed exchange of mass at the trailing edge. Heller and Bliss formed this into a six step process describing the oscillation feedback cycle described using their pseudo-piston model which can be seen in Figure 2. They claimed that their analytical model could predict mode shapes which they backed up with experimental data but no actual equation of the model.

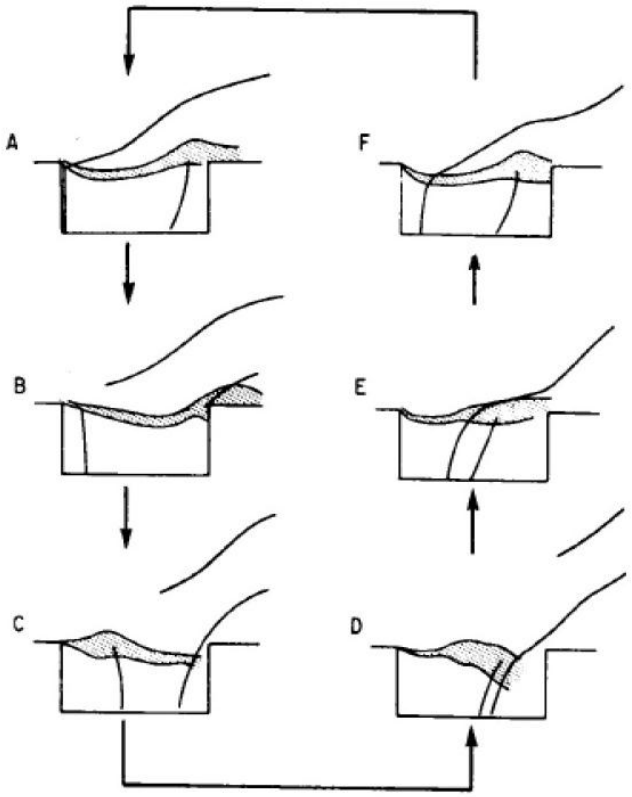

Figure 2- Cavity Pseudo-piston Oscillation Cycle. (from Heller and Bliss [1])

Unlike many before them, Tam and Block [9] looked at cavity flow from a different perspective, focusing on the low subsonic range in creating their model of cavity flow. They formed their own mathematically rigorous cavity model to predict cavity frequencies based on momentum thickness θ and were the first to account for acoustic reflections from the cavity floor and front wall, factors which they proved were important to an accurate model. They were also the first to realize the importance of not only L/D in predicting cavity behavior but also θ/L, momentum thickness of shear layer to length ratio.

As the field of cavity flow continued to grow and expands its understanding, it became obvious that certain divisions and classifications could be applied to identify particular types of cavity flow from others. In 1978, Rockwell and Naudascher [2] categorized self-sustaining oscillations into three groups based on their flow behaviors: fluid-dynamic, fluid-resonant and

fluid-elastic. Fluid-dynamic is where oscillations come from the flow's inherent instability while those from fluid-resonant are influenced by resonant wave effects or standing waves. Finally, fluid-elastic is where the oscillations are coupled with an 'elastic' or moving, solid boundary. These three classifications and the various types of cavies that fall under each can be seen in Figure 3. For the purposes of this study we are only interested in the fluid-resonant category, as it can be further subdivided into three types of cavities based on the length to depth ratio. Each type, open, closed and transitional, describes a different stage in cavity flow as the L/D changes.

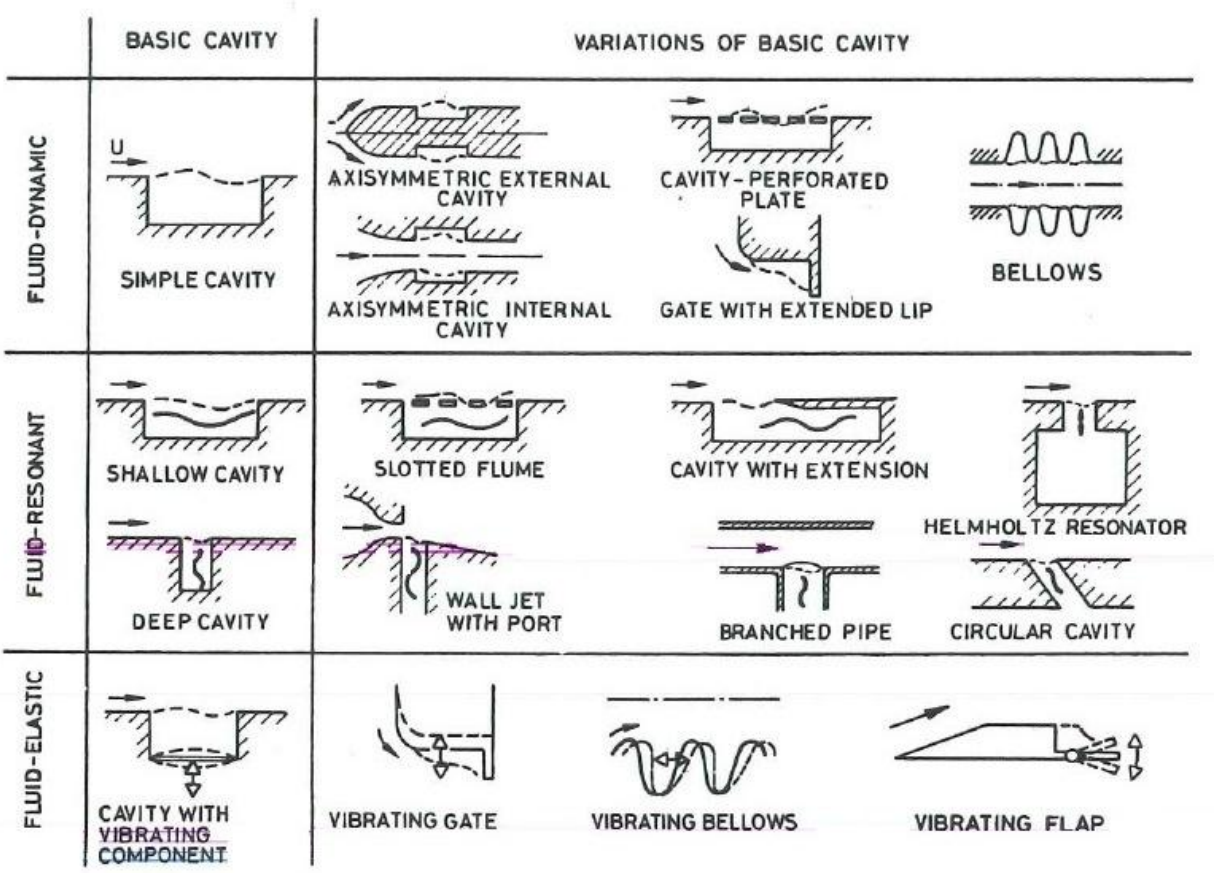

Figure 3- Categories of Fluid Cavities. (from Rockwell and Naudascher [2])

Plentovich, Stallings and Tracy [3] described each of these types of flow and defined the ranges of *L*/*D* at which each occur. Images of each type can be seen in Figures 4-6.

- Open Cavity Flow: An open cavity flow occurs when a shear layer is formed and spans the entire cavity without attaching to the cavity floor. The range of *L*/*D* this generally occurs at is less than or equal to 10.

- Closed Cavity Flow: A closed cavity flow occurs when, instead of forming a shear layer, the flow separates at the leading edge and attaches to the cavity floor. It then separates again before reaching the rear cavity wall. Closed cavity flows occur at an *L*/*D* of roughly greater than or equal to 13.

- Transitional Cavity Flow: This type of flow falls between open and closed cavity flow and can be divided into open transitional and closed transitional. In a closed transitional flow, the impingement shock and the exit shock from a regular closed cavity flow, as seen in Figure 5, are combined into one single shock signifying that the flow has impinged on the cavity floor. An open transitional flow is similar, but instead of a single shock a compression wave is formed, as can be seen in Figure 6. Since this category falls between open and closed flows, the *L*/*D* range is generally between 10 and 13.

This study will be focused entirely on open cavity flow, as this is the range of *L*/*D* into which cavities for most applications fall.

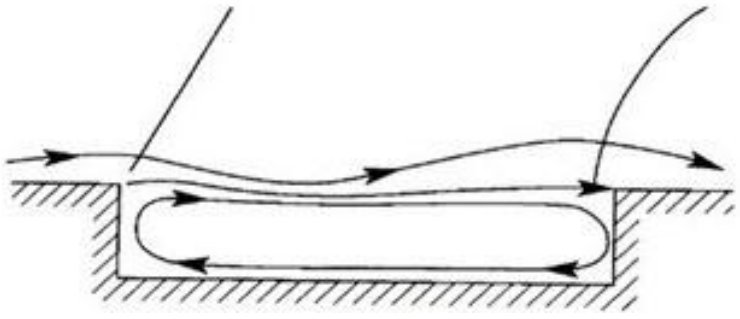

Figure 4- Open Cavity Flow, *L*/*D*<10. (from Plenovich, Stallings and Tracy [3])

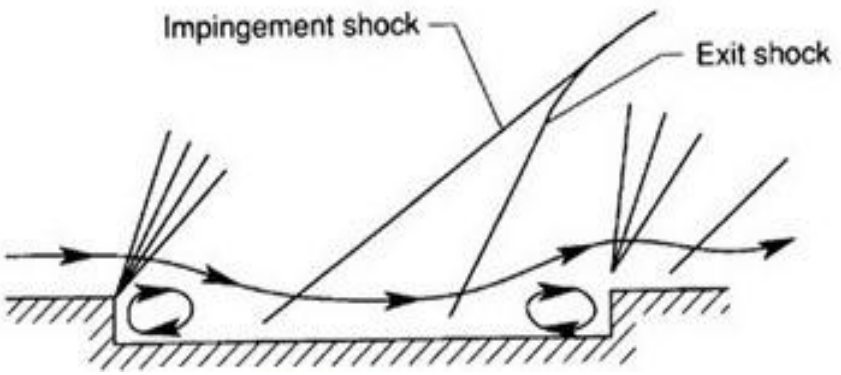

Figure 5- Closed Cavity Flow, *L*/*D*>13. (from Plenovich, Stallings and Tracy [3])

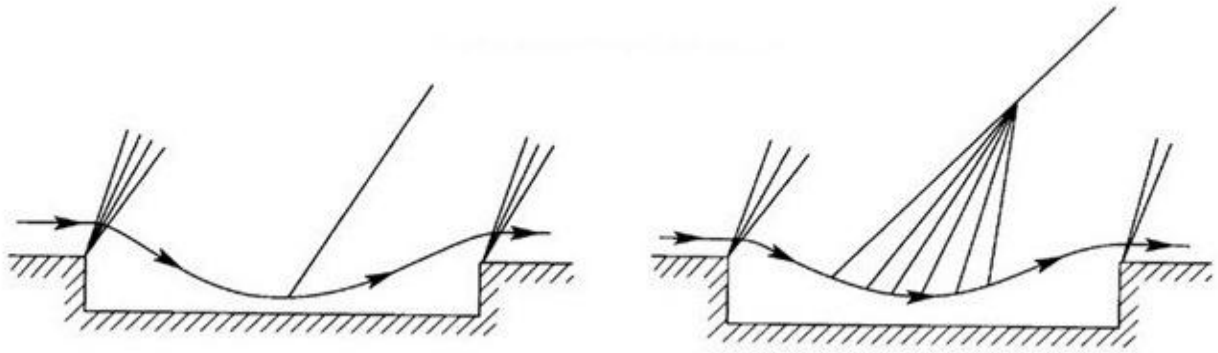

Figure 6- Transitional Cavity Flow, 10<*L*/*D*<13. (from Plenovich, Stallings and Tracy [3])

Classifications based on *L*/*D*, such as those just discussed, inherently imply a cavity of uniform geometry, and up until recent years the study of cavity flow has used rectangular cavities almost exclusively for testing. While they may not be as accurate as a more complex geometry, a rectangular cavity can be more universally applied to a broader range of problems, as well as being much easier and cheaper to manufacture. But we have now reached a point where the study of three-dimensional cavity effects due to irregular geometry has become important, and studies have started looking at not only general three-dimensional cavity effects but also specific scale cavity models such as the tests on the $1/20^{th}$ scale F-111 weapons bay model [10]. Other studies, like the one conducted by Ukeiley, Sheehan, Coiffet, Alvi,

Arunajatesan and Jansen [11], focused on studying realistic three-dimensional flow in a less specific, but no less complex, cavity with angled side walls and a sloped floor.

The study of cavity flow is still growing as many new topics have become available which weren't previously possible. The complex cavity geometries discussed above are one example, but with the constant advances in technology over recent years, many new tools have become available. These tools can be used to analyze cavity flow and allow a greater understanding of what is occuring inside a cavity than was previously available. One of these new tools often used in modern studies is Particle Image Velocimetry (PIV). This flow visualization technique can be used to visualize velocity and vorticity fields inside a cavity. In a study conducted by Ukeiley and Murray [12], PIV was used in conjunction with pressure and hot-wire measurements to provide more information to support the existence of different cavity modes.

Another relatively new addition to the study of cavity flow is Computational Fluid Dynamics (CFD). This is a method of computationally modeling a system without physically having to run an experiment. While the details of how CFD works are beyond the scope of this review, how it is utilized for the purpose of studying cavity flow will be briefly discussed. Until recently, cavity flow research has relied entirely on experimental data to understand and learn about the flow mechanisms. While CFD modeling will not replace experimental studies, it can be used as a quicker and cheaper method to get a general idea of what is going on in a flow. Not only this, but by working to develop models which agree with experimental data more accurately, we are forced to understand and learn about the core flow mechanics. Arunajatesan, Kannepalli, Sinha, Sheehan, Aliv Shumway and Ukeiley [13] used CFD to do just this, gaining insight into the governing flow mechanisms and comparing the results to experimental data. The study of cavity flow is not just a thing of the past and is still happening as we continue onto deeper studies beyond that which the founders of this field were capable.

Since the study of cavity flow began, much has happened to allow us to understand and define it, as described in this section. But as was previously mentioned, this chapter is only a brief review of some of the most important discoveries and foundations of cavity flow. Its purpose was to give both a basic understanding of what we have come to know about cavity flow and an idea of how much there is yet to learn.

2.3 Cavity Flow Control Review

The study of cavity flow came about due to the desire to be able to negate the potentially destructive forces created by a cavity's presence. Therefore it was natural that part of that study would be focused on not only understanding cavity flow but finding methods to control it. This is called cavity flow control. But since different cavities react to different circumstances, it was inevitable that many different methods of approaching flow control would be proposed over the years. Out of these various approaches grew a system of classification based on how the different methods went about their control. Cattafesta III, Williams, Rowley, and Alvi [14] describes these as "passive" and "active" flow control, where active is defined by the fact that it provides an external energy to the flow, while passive only works to alter the flow's existing energy. Active flow control can also be divided into two more branches called open-loop and closed-loop. Closed-loop is defined by the existence of a feedback loop for control, while a control method that doesn't have a feedback loop is considered open-loop. Active, closed-loop control is outside the scope of this thesis but the reader is referred to the work by Cattafesta, et al. who details this subject further. This review will be concerned with only passive and active, open-loop cavity flow control methods and while it cannot contain the extent of the literature covering this topic, the following review is sufficient to put the current study in proper perspective.

Some of the earliest attempts to control cavity flow fall under the category we now call passive flow control. Rossiter [7] was one of the first in 1964, using spoilers at the leading edge of a cavity with $L/D = 1$ to reduce pressure fluctuations. He varied the height and width of the spoilers (as can be seen in Figure 7), and his results showed that, while the presence of any spoiler would decrease the pressure fluctuations, the larger the spoiler the better the results.

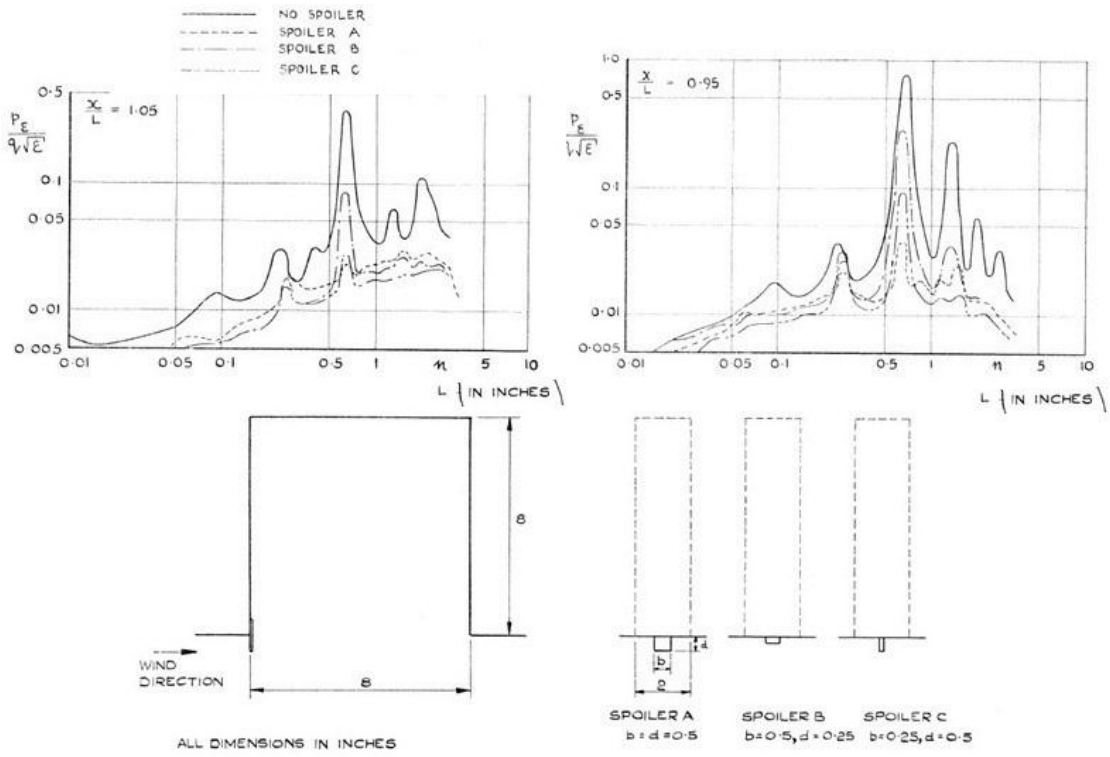

Figure 7- Spoiler Designs and Amplitude Spectra at M = 0.9. (from Rossiter [7])

When Heller and Bliss [1] started looking at suppression techniques based on their newly formed model, they acknowledged that stabilizing the shear layer through the use of vortex generators or spoilers was one method. But considering their cavity model, with trailing edge mass flow fluctuations, they proposed another passive method which could be used alone or in tandem with the previous method. They tested a cavity where the rear cavity wall had a 45° slant, both with vortex generators and without. Their results showed that the slant did reduce pressure levels and even more so when used in conjunction with the upstream vortex generators. The maximum reduction was roughly 25 dB, a measure of what is called the Sound Pressure Level (SPL).

$$\mathrm{SPL} = 20\log_{10}\left(\frac{P_{\mathrm{rms}}}{P_{\mathrm{ref}}}\right) \qquad (3)$$

In this equation P_{rms} is the root mean square pressure and P_{ref} is a reference pressure equal to 20 microPascal (μPa). SPL is a measure of the sound pressure or 'magnitude' relative to a reference, and it's the most common form used to compare and describe pressure fluctuations in cavity flow.

In the same year, Franke and Carr [15] worked on testing a large number of geometric cavity alterations to see which ones would affect pressure fluctuations and how much. They first did water table testing on several dozen different cavity configurations, before doing air flow tests with the cavities which showed the best results. Some of the variations tested were ramps, baffles, airfoil shaped spoilers, double cavities and combinations of each. In the end it was concluded that while results varied a lot depending on cavity size and Mach number, the 'double ramp' or ramps on both the leading and trailing edge were the most effective.

While most of the early studies in cavity flow control focused on passive control such as spoilers and ramps, the severe limitations to which they were subject eventually became obvious. While it was shown in the studies mentioned above how well these methods could work, they usually were only so successful at slower speeds and at certain cavity *L*/*D*. As supersonic applications became increasingly important, so did the need to find a reliable method of flow control that would provide the same results spoilers and ramps had for slower speeds. Additionally, any new methods couldn't introduce a large drag penalty when used at supersonic speeds, as would naturally be created by a spoiler.

One major type of active flow control which hoped to address these issues and has become quite popular over the years is high frequency forcing. This method attempts to decrease pressure fluctuations by stabilizing the shear layer directly at the smallest scales of vortical structures instead of indirectly through large scale vortical structures. Wiltse and Glezer [16] used cantilevered piezoelectric actuators to force the flow at a frequency roughly a magnitude lower than the passage frequencies of eddies. They hoped that by directly exciting the small scales, energy would transfer from larger to smaller scales faster, as well as increase dissipation and the decay of turbulent kinetic energy. Using hot-wire measurements they were able to conclude that dissipation did increase when the flow was forced by more than an order of magnitude, showing that the excitation was causing an energy transfer from larger to smaller scales.

This concept was picked up by Stanek and a number of collaborators [17, 18] who formulated their own model of how high frequency forcing was affecting the shear layer. They said that this model was more consistent with experimental results, physical reality and the classic theories of turbulent flow. Wiltse and Glezer [16] had claimed that their measurements proved that frequency forcing created a cascade effect with decreased energy in large scales and increased energy in small scales. But Stanek, et al. claimed that instead the reason for these results was not from an energy cascade but from less turbulent kinetic energy being produced in the first place. Their model changed high frequency forcing from a shear layer dissipation technique to a shear layer stabilization technique.

Following this work Stanek, Ross, Odedra and Peto [19] began looking into the use of a leading edge, cylindrical rod in crossflow as a method for high frequency forcing. Unlike previous methods of frequency forcing, this one used a passive control technique in a stationary rod instead of an active one such as the piezoelectric actuator used by Wiltse and Glezer [16]. The study claimed to be the first to unequivocally link an increase in acoustic suppression with high frequency shedding due to the rod configuration. Various placement and sizes of rods were tested, and Stanek, et al. were able to obtain a subsonic suppression of roughly 10 dB and in supersonic tests a reduction of around 16 dB.

Despite the absolute certainty of Stanek, Ross, Odedra and Peto [19] in the reasoning behind the suppression obtained using a rod in crossflow, there was still much debate regarding this technique. Many thought that lofting and blockage effects similar to other passive techniques such as spoilers were the large part of the suppression results obtained instead of high frequency forcing, as was typically expected from an active actuating method. The reader is referred to the thesis works of Loewen [20] and Fowler [21] who explore this subject further.

Another active cavity flow control technique which has gained a lot of popularity due to its promising results is mass-injection. This occurs when mass flow is introduced or re-introduced into the flow in such a way as to alter the flow properties. There are many different examples of mass-injection, but they can all be categorized into one of three types according to Fernandez and Zukoski [22].

- Weak Mass-Injection: For this type of mass-injection, the momentum of the flow being injected is so small compared to skin friction that it only really interacts with the boundary layer, slowly increasing it over a long distance. The flow outside the boundary layer, external flow, is barely altered.

- Massive Mass-Injection: Unlike the previous type of mass-injection, this one interacts a lot with the external flow. This time, the momentum of the injected flow is large compared to the skin friction, but still not as large as the momentum of the external flow. It lifts the boundary layer and external flow upwards and forms a layer where they mix with the injected flow.

- Blow-Off Mass-Injection: In this last type of mass-injection the momentum of the injected flow is so large that is comparable to the momentum of the external flow. When this happens the injected flow doesn't stay near the wall and gets blown out into the external flow just like a jet.

Placement and proper use of mass-injection has been studied extensively, looking for the best way to use mass-injection as a form of cavity flow control. In 1977, Sarohia and Massier [23] looked at the effects of mass injection introduced along the length of the floor of two axisymmetric cavity models. Their hope was that, by providing mass injection at the base of the cavity, it would prevent the cavity trailing edge mass exchanged postulated by Heller and Bliss [1] and thereby eliminate the shear layer oscillations which causes undesirable cavity noise. They concluded that continuous mass-injection did have a stabilizing effect on the shear layer, decreasing the SPL by roughly 10-12 dB, but that approximately 5 to 15% of the freestream mass flow would be require to suppress cavity flow noise.

Not all methods of mass-injection require adding large amounts of extra air into the flow though. Sometimes it can be just an exchange of flow from one part of the cavity to another. This more passive method was studied by Wilcox [24] who placed a porous floor inside a cavity with a venting chamber beneath. The purpose was to allow high pressure flow from the rear of the cavity to vent to the low pressure regions towards the front part of the cavity. Wilcox concluded

that the porous flood was extremely effective for closed flow cavities, decreasing drag and even modifying the flow from closed or transitional closed to transitional open.

Other early attempts at finding the best positioning for the more traditional method of mass-injection include tests done by Franke and Sarno [25]. They used static and pulsed mass-injection at the leading edge, both parallel to the flow as well as at a 45° angle. Their results showed that for static tests injecting at an angle provided a maximum reduction of roughly 10 dB at a mass flow rate of 1.05 $lb_m/s/ft$ while the parallel injection only reached roughly 5 dB at 1.5 $lb_m/s/ft$ mass flow rate. For the pulsing mass-injection tests, pulse frequencies ranging from 0 to 80 Hz were looked at, but they showed little effect on suppression.

One of the first studies with major results was the upstream mass-injection study by Vakili and Gauthier [26]. The purpose of the study was to control the boundary layer thickness ahead of the cavity as well as the cavity shear layer using relatively low injection mass flow rates. Two different configurations were tested, both using perforated plates with 175 holes, but one had a high density of injection holes while the other had a low density as can be seen in Figure 8. Considerable reduction in flow oscillations were measured for the low density configuration with a decrease of 27 dB. This was attributed to the thickening of the cavity shear layer which was measured when mass-injection was used compared to when it was not.

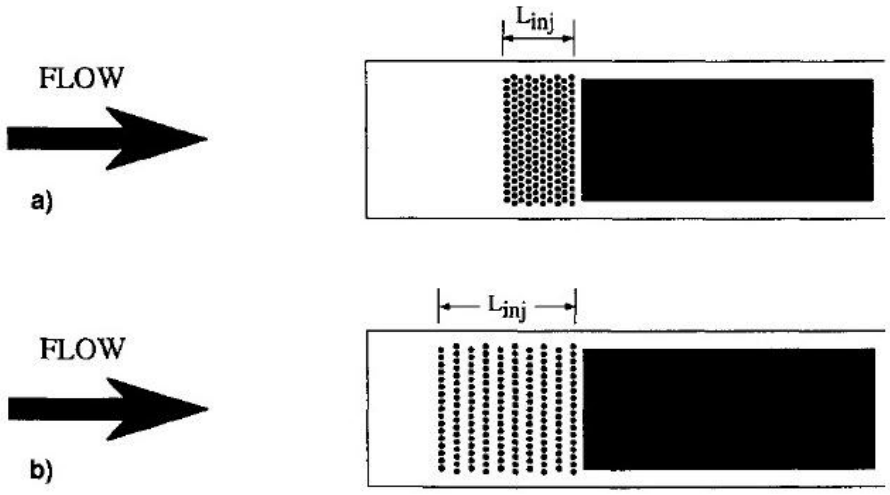

Figure 8- Mass-Injection Perforated Plate Density. (from Vakili and Gauthier [24])

In 2012, Milne [4] did a study using the upstream mass-injection concept put forth by Vakili and Gauthier [26], but instead of using mass-injection, an active flow control method, passive vertical rods were used. The idea was that small cylindrical pins placed vertically in the upstream flow would interact similarly to the upstream mass-injection. Milne tested many different configurations with varying pin heights and density of placement to determine not only if the concept worked, but the best possible configuration for maximum suppression. Using proper pin distribution, suppression of up to 23 dB was obtained, almost as much as that observed by Vakili and Gauthier. Despite this promising result the role of pin density was inconclusive and required further study. However, it was determined that of the pin heights tested the tallest, ½ inch, obtained the best results. The exact cause of this is undetermined, but it may be due to the fact that unlike the shorter pin heights tested, the ½ inch pins extended slightly above the boundary layer which was calculated for this cavity and flow speed to be roughly ⅜ inch thick by Fowler [21].

CHAPTER 3- EXPERIMENTAL PROCEEDURES

3.1 Introduction

This chapter contains a complete description of the University of Tennessee Space Institute's (UTSI) High Speed Wind Tunnel (HSWT) and its components. This will be followed by an explanation of how Particle Image Velocimetry (PIV) works and the equipment used to run it. Next is discussed the systems used to acquire the PIV data and the theory behind them, as well as post-processing techniques for validating and presenting the data. Then a discussion will be included of the various test configurations used in this study and why they were chosen.

3.2 High Speed Wind Tunnel Apparatus

The High Speed Wind Tunnel used for this study was a blow-down configuration fed by an external compressor. This compressor pressurizes an outdoor tank farm which consists of 18 high pressure cylinders to a maximum of 3000 pound/square inch (psi). When the HSWT is in use, air is routed through a pneumatically driven ValTek FlowServe valve which controls the mass flow rate allowed to reach the tunnel. This valve is controlled using LabVIEW software run on a computer by a UTSI lab technician and is generally set for a mass flow rate of 26 pound/second (lb_m/s).

The air is then fed into a plenum, or stilling chamber, which has four stages filled with a series of honeycomb grids and screens for the purpose of creating a uniform flow as it approaches the test section part of the tunnel. First the flow is driven through a converging/diverging nozzle which allows for control of the flow's velocity in the testing area. Currently the nozzle is configured to reach a Mach number of 1.85 in the test section, but in practice, once the flow through the nozzle throat has become choked the flow is actually moving at closer to Mach 1.84. This, along with several other important flow parameters, such as local speed of sound and the freestream velocity, were calculated based on the measured total pressure and temperature in the stilling chamber and the static pressure in the test chamber. Table A.1 in the appendix shows the values of these parameters and the equations used to calculate them.

The test section itself is a 4 foot long, 8 inch by 8 inch, square duct fitted with quartz glass observation windows allowing for image based testing applications such as Particle Image Velocimetry. The test section contains several dynamic pressure transducers which can collect spectral data during tests runs. These high sensitivity miniature pressure transducers were Kulite® model XCS-133-093-15D. This model of pressure transducers is quoted to have a full scale output (FSO) of 200 mV for our pressure range with an accuracy of ±0.1%.

Once the air leaves the test section, it is diffused out into atmospheric conditions. A diagram of this complete system is detailed in Figure 9, including the additional apparatus required to run the PIV system which will be discussed in the following section.

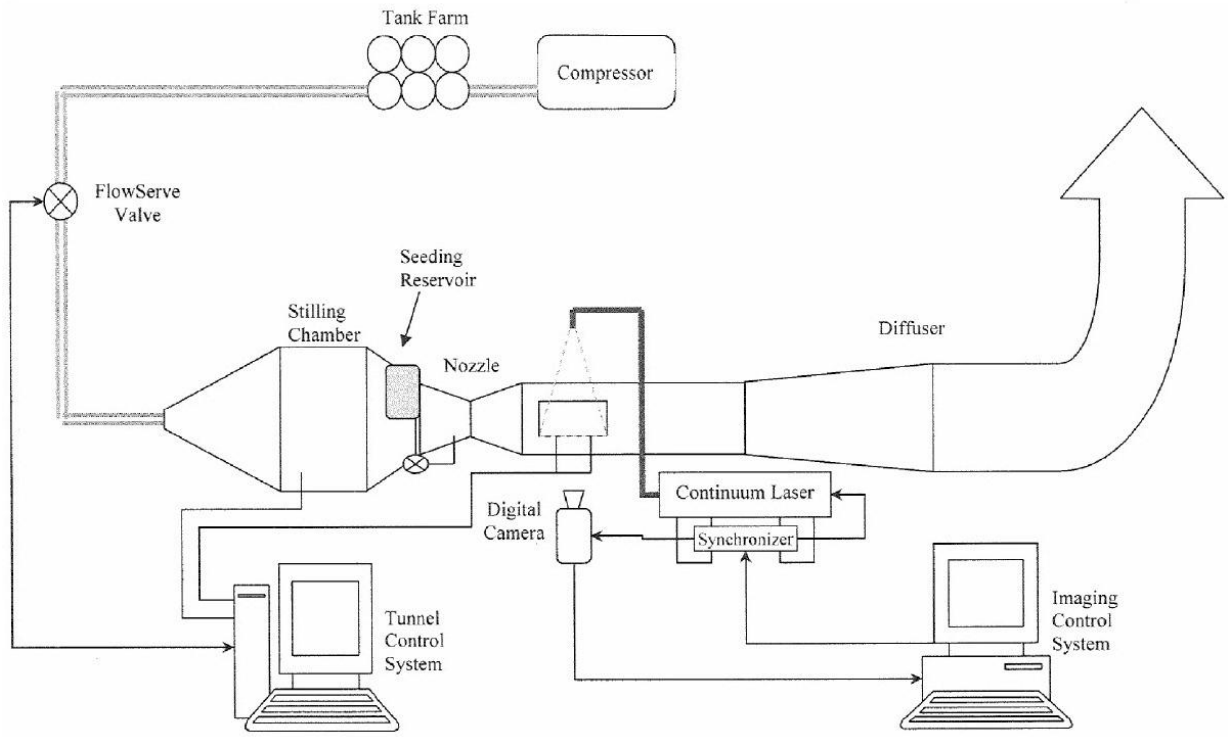

Figure 9- HSWT with PIV Apparatus. (from Loewen [20])

3.3 Particle Image Velocimetry Technique

Particle Image Velocimetry (PIV) is a non-intrusive method of visualizing a flow field and calculating the flow's velocity vector field. This is accomplished with the use of high powered lasers which are formed into a sheet of light and directed into the HSWT test chamber. Here the flow is filled with "seeds", atomized particles of a dye mixture, which were introduced into the flow upstream. This dye must be carefully chosen and controlled so that once atomized into the flow, the seeding particles won't be so large that they could alter the natural flow of air, thereby interfering with any results trying to be obtained. It also must be a dye which will fluoresce when the laser light hits it. This allows a camera to pick up an image of the particles at that moment the laser is directed into the test chamber. If the laser is then pulsed twice, and the camera is synchronized to take a picture at each moment the test section is illuminated, the progression of the seed particles can be captured. Using methods which will be discussed in a later section, the particle displacement, dx, can be calculated from this image pair. Combining this particle displacement and the known laser pulse separation time, dT, it is possible to calculate the flow velocity field in the test section at the moment the laser was pulsed.

The TSI LASERPULSE PIV system has been configured for use with the HSWT tunnel using two Continuum Nd:YAG (neodymium-doped yttrium aluminum garnet) lasers. The laser beams reach the test section by reflecting through a series of carefully positioned mirrors in an articulating laser arm. It is at the end of this arm that the beam is then directed through a pair of lenses which are pictured in Figure 10. A cylindrical lens is used to expand the beam into a plane in which a spherical lens is positioned to focus the plane into a thin sheet of laser light which illuminates the test section.

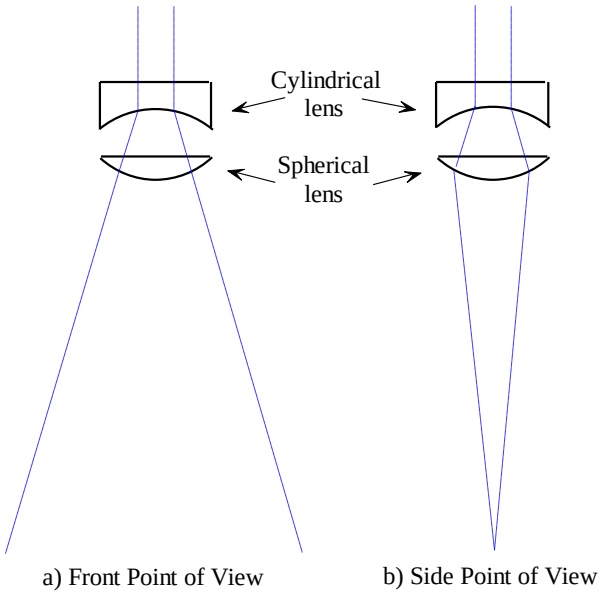

Figure 10- Sketch of PIV focus lenses.

A machine called a Synchronizer has the job of being the timing master of all the components, controlling how the camera works in conjunction with the laser to assure that images are captured exactly when required. The CCD (charge-coupled device) camera itself is specifically intended for use with a PIV system, capable of 30 frames per second, and uses a wide angle 28mm F/2.8 Nikkor lens. For this study the camera aperture was set to F5.6. A value chosen for the light intensity distribution it provided to the images being captured.

The final pieces of equipment needed to successfully use PIV are those necessary to introduce the seeding to the tunnel flow. Attached to exterior of the converging/diverging nozzle is a small cylindrical capsule which acts as a reservoir for the dye mixture used in PIV for seeding. The dye is created from a combination of diluted isopropyl alcohol (70% isopropyl and 30% water) and fluorescein, a common type of laser dye. This mixture is dispersed into the flow using a shop hose. The hose brings low pressure air into the capsule which acts as the means to propel the seeding into the flow, a process which is controlled using a pressure regulator and manual valve. The air driven seeding reaches the tunnel flow through tubes which run from the control valve into a ⅛ inch spray bar which is inserted at the bottom of the converging part of the

converging/diverging nozzle, about a foot ahead of the throat. This placement allows enough time for the seeding to atomize and disperse evenly before reaching the test section, even at supersonic speeds. The spray bar consists of two concentric cylindrical pipes, one with the dye mixture fed from the regulator valve through the previously mentioned tubes and the other with pressurized air diverted directly from the shop hose through a different set of tubes. The pressurized air propels the dye forward to be atomized and mixed into the flow. The spray is actually directed upstream, into the oncoming flow, to help improve the uniformity of the atomized seeding, a parameter that will play into the accuracy of our results.

3.4 PIV Software and Post Processing

The core of the TSI LASERPULSE PIV system is the control system which uses INSIGHT^{TM} PIV Software. This allows you to configure the settings to your specific testing needs. From this interface you can control all aspects of the system such as the laser pulse separation time, laser intensity, the number of image pairs desired, camera exposure modes, correlation schemes, and more. All of these settings affect how the system goes about calculating the vector field and how accurate its results will be.

The INSIGHT software uses a correlation scheme called cross correlation to calculate the velocity vectors for each image pair taken by the camera. The cross correlation process consists of determining the change in position in both the *x* and *y* directions during the laser pulse separation time, dT, and calculating velocity from it. This is accomplished by dividing the image into smaller sections called interrogation regions. The size of these regions is a user input called spot size, the value of which is equal to the number of vertical and horizontal pixels in one interrogation region (aspect ratio of one). A common rule of thumb in deciding the correct spot size to use is that the maximum expected distance traveled by particles during the laser pulse separation time should be roughly a fourth of the correct spot size. The possible spot sizes offered by INSIGHT are 32, 64 and 128 pixels. According to several test conducted by Fowler [21] in the UTSI HSWT at Mach 1.84, the best tradeoff between strong correlation and

reasonable variation between velocity vectors can be obtained using a dT of 2 microseconds (μs) with a spot size equal to 64 pixel. These are the settings which were used for this study.

One of the issues with the cross correlation process is the limitations of digital cameras, namely the image capture rate. To ensure the movements of the particles in the flow are captured correctly, it is necessary that the laser pulse separation time be extremely small, especially when used with supersonic flows. The number of frames per second that even a high speed digital camera is capable of capturing is limited, making cross correlation an impractical method to use if not for a technique called frame straddling. This technique dictates that the first laser pulse falls at the end of the camera exposure time while the second laser pulse occurs at the beginning of the exposure time, as can be seen in Figure 11. Since we cannot shrink the camera exposure time we have shifted the timing of the laser pulses to still allow for two images to be taken with an extremely small separation time.

One final step in preparing to run INSIGHT is a velocity calibration. When the cross correlation technique calculates velocity it measures the distances traveled by particles in number of pixels. To calculate velocity in units such as meters per second INSIGHT requires a conversion factor. We can obtain this conversion factor using the INSIGHT velocity calibration setup. Here there is the option to indicate the size of an object seen by the camera and measure the number of pixels corresponding to this size. From this the conversion factor can easily be obtained. Since this process is entirely based on the camera's current position and field of view, any time the camera is moved or positioned differently a new calibration must be done to obtain the new conversion factor. For this study two different camera positions were used and therefore two different calibrations were run.

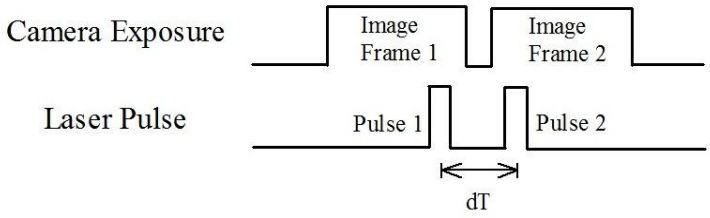

Figure 11- Frame Straddling Exposure Technique.

Once the settings and calibration are completed, the system is ready to capture as many image pairs as you indicate. For this study 120 image pairs were recorded for every HSWT run to allow for more accurate results. Once the images are captured the cross correlation process can be applied to calculate the velocity vector field for each image pair. After this has been completed it is necessary to put the vectors through post-processing. Whether from a high gradient in your flow or particles moving outside the bounds of the interrogations areas, a certain amount of spurious, or bad, vectors will appear in your results. These vectors must be dealt with in order to obtain an accurate vector field. INSIGHT has built in post-processing options which can be used to validate either a single vector field file or an entire batch. For this study Gaussian smoothing was used to eliminate erroneous vectors and interpolate what the vector in that location might have been based on the surrounding vectors.

After completing the post-processing the velocity vector data files can be imported into Tecplot software for the purpose of plotting the vector fields and contours plots, as well as calculating other pertinent variables. One such variable is vorticity ω which is calculated from the derivatives of the *x* and *y* components of the local velocity, *u* and *v*, using a Tecplot macro according to equation (4). The factor of 2 in the denominator is needed to account for the spatial geometry of the grid setup.

$$\omega_z = \frac{\left(\frac{\partial v}{\partial x}\right) - \left(\frac{\partial u}{\partial y}\right)}{2} \qquad (4)$$

In order to be able to directly compare data from one configuration to the next it was useful to convert both the velocity and the vorticity into their non-dimensional forms. Following the same format as previous studies by Meganathan [27], Radhakrishnan [28], Loewen [20] and Fowler [21], the non-dimensionalized local velocity magnitude U^* was obtained using the local velocity magnitude U and the freestream velocity U_∞, as show below.

$$U^* = \frac{U}{U_\infty} \qquad (5)$$

Similarly, the non-dimensional vorticity ω^* was calculated using the cavity depth D and the freestream velocity U_∞.

$$\omega^* = \frac{\omega D}{U_\infty} \quad (6)$$

It is these non-dimensional variables which will be shown in all plots following in Chapter 4.

3.5 PIV Measurements Error Analysis

An interrogation spot size of 64 x 64 pixels was used for all PIV images used to determine the velocity field. The distance between any two adjacent vectors was 25 pixels horizontally and 6 pixels vertically with an image calibration of 127.4 μm/pixel for all cases. The resolution of the vector field can be calculated based on this and is 3.185 millimeters horizontally and 0.7644 millimeter vertically. These values can then be used to determine the minimum vortex structure size that can be visualized. To do this, first we have to determine how many data points are needed to determine a structure. If we say that at least 3 x 3 vectors are the number of vectors needed to properly resolve a vortex structure, then using the larger, horizontal vector resolution, we could identify all structures above a diameter of roughly 6.270 millimeters.

The primary form of error that will be discussed here is computational error, namely in the velocity. These computational errors include those from truncation, detection and precision error and are discussed in more detail in the error analysis section of the study done by Meganathan [29]. In this study he states that the uncertainty in the subpixel interpolation is about ±0.1 pixels. Using this along with the freestream velocity, U_∞, in the current study and the separation time between images, dT, the error in the maximum velocity can be calculated to be roughly ±1.38%. Meganathan [29] also describes the method of determining the error in the derivatives used to calculate vorticity from the velocity and position data. This error has two components; the truncation error is on the order of Δx^2 and the uncertainty in the velocity of the order $1/\Delta x$.

Meganathan [29] also describes the error in resolving position and velocity using the analysis method described by Adrian [30]. Here he details how to obtain two non-dimensional quantities

called Dynamic Spatial Range (DSR) and Dynamic Velocity Range (DVR). DSR is defined as the field-of-view in the object space divided by the smallest resolvable spatial variation and for this study came out to 127.953, while DVR is the ratio of the maximum velocity to the minimum resolvable velocity and it was calculated to be 20.693. These two variable expressions can also be combined to obtain another non-dimensional quantity which defines the capability of a PIV system to have both a large dynamic velocity range and a large spatial range. For this study a value of 2647.731 was obtained. PIV systems having large values of this combined DSR and DVR quantity are well suited for turbulence research, and measurements in higher Reynolds number flows too require larger values of this constant. Typical values of this constant ranges from a few thousand for standard video to several hundred thousand for high-resolution films. The reader is referred to the two previously mentioned papers for further information on analyzing dynamic PIV resolution error, using these variables as well as the details of how they were calculated.

3.6 Test Configurations

In this study four pin configurations plus an empty baseline were tested. These configurations were chosen due to being the most successful at acoustic suppression based on the results of Milne [4], who tested a large number of configurations which varied both in patterns of pins and pin heights. Figure 12 displays diagrams for the pin locations for each of the configurations tested. A solid circle indicates the location of a pin, and a hollow circle indicates an empty pin hole. All of the pins used in these configurations had a height of ½ inch above the surface of the pin plate and a diameter of ⅛ inch.

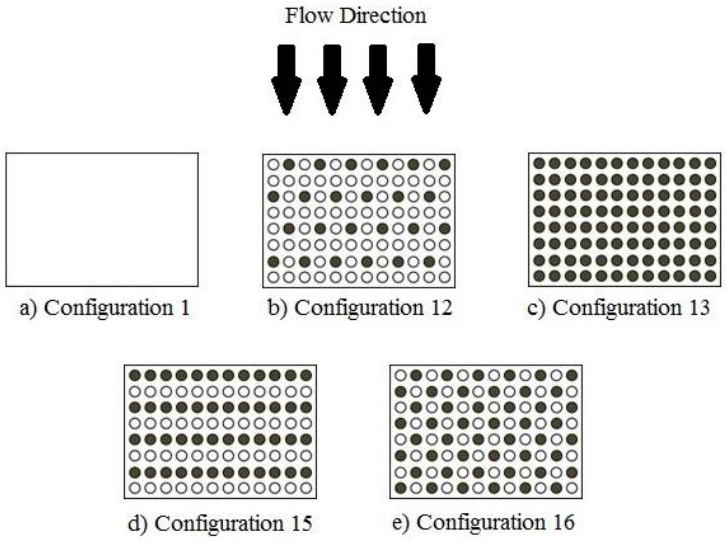

Figure 12- Test Configurations.

- Configuration 1- Baseline: This configuration utilized a flat empty plate insert as can be seen in Figure 12 a) to simulate an unaltered leading edge surface. This creates a blank cavity with no flow control being applied to use as a baseline for comparison with all further data.

- Configuration 12- Staggered Every 2nd Row: This configuration utilized the pins which extended above the surface of the plate by ½ inch, the tallest pin height tested by Milne [4]. Shown in Figure 12 b), it had the least number of pins of all those tested in this study, yet its staggered pattern still presents no large gaps where flow can easily pass unperturbed. While this resulted in the smallest decrease in sound pressure level (SPL) in the important second mode according to data obtained from Milne, it can be seen in Table 2 that this configuration had the largest decrease in overall SPL of the four configurations compared.

- Configuration 13- Full plate: Once again using all ½ inch pins, this configuration had the most number of pins with the whole pin plate being filled up. This presented the flow with the most concentrated mass of pins of the configurations tested. It could be said that

this configuration had the smallest effect on the flow, with Table 2 showing the smallest overall change in SPL and the second smallest SPL decrease in mode 2.

- Configuration 15- Every other row open: With the second largest change in SPL, both for mode 2 and the overall this configuration was once again very important to study to further understand how the pins were interacting with the flow. Also using ½ pins, this configuration presented a solid front similar to the full plate and unlike the staggered configurations, but allowed for gaps between rows as pictured in Figure 12.

- Configuration 16- Staggered Row-to-Row: Despite having the second lowest overall change in SPL, this ½ inch pin configuration was an important one to test as it had the largest SPL change for mode 2 of all configurations tested by Milne [4]. This made it a key configuration to examine further in this study. As can be seen in Figure 12 e), this configuration has the staggered pattern of configuration 12 but doesn't quite have the solid mass of pins that the full pin plate presents to the flow.

Table 2- Sound Pressure Level Change for Tested Configurations.

	Mode 1 Change in SPL (dB)	**Mode 2 Change in SPL (dB)**	**Mode 3 Change in SPL (dB)**	**Mode 4 Change in SPL (dB)**	**Overall Change in SPL (dB)**
Configuration 12	16.97	20.01	15.66	23.3	75.94
Configuration 13	13.43	20.15	13.33	15.15	62.06
Configuration 15	13.6	21.22	14.4	18.84	68.06
Configuration 16	14.85	23.17	12.29	16.6	66.91

CHAPTER 4- EXPERIMENTAL RESULTS AND ANALYSIS

4.1 Introduction

In this chapter a discussion of the observed results found for each of the tested configurations will be presented. The order of configurations to be discussed will begin with a "clean" tunnel with no cavity or control methods, followed by the baseline empty cavity and the four pin configurations in order according to the configuration numbers assigned by Milne [4] and which can be seen in Table 1. The discussions for each configuration will include outlining the configuration layout and presenting the acoustic spectral data, followed by observations about the configurations based on the velocity vector field, as well as the average and instantaneous contour plots for velocity and vorticity. Figure 13 provides a frame of reference for the field of view used in these tests. This is the same field of view which will be used for all following contour plots and as indicated in Figure 13 the flow direction is from left to right. The axes are non-dimensionalized by the cavity length with the origin located at the cavity leading edge. All contours shown will be plotted using the same axes.

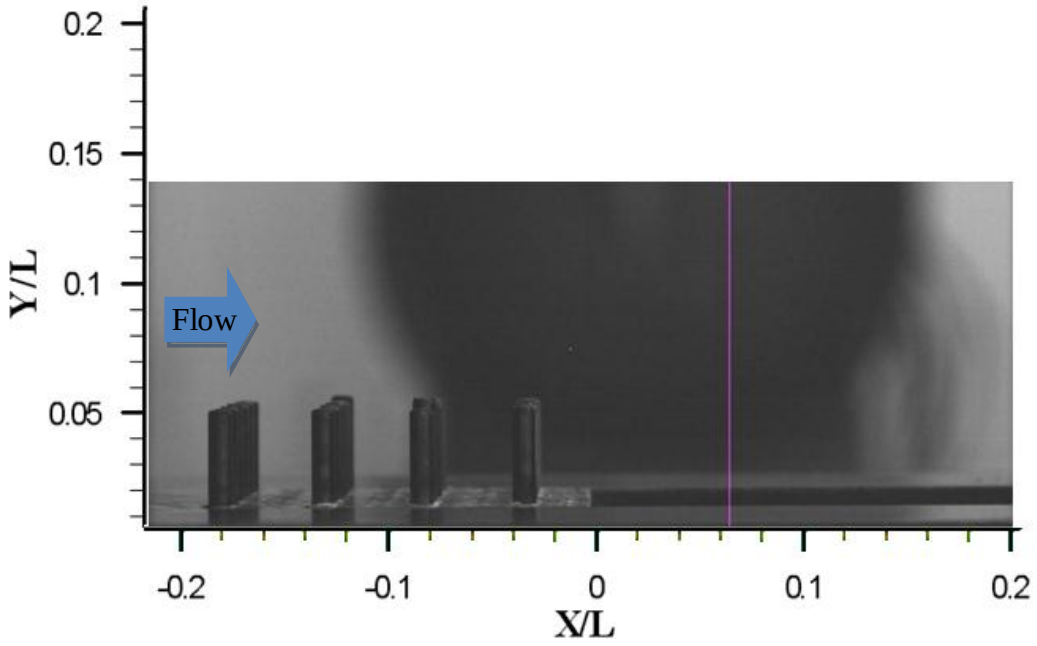

Figure 13- PIV Field of View Reference with Non-Dimensional Axes.

4.2 Clean Tunnel

As a pre-cursor to testing even the baseline cavity, it is desirable to know the amount of noise which is caused purely by the tunnel itself, with no cavity present. This is an experimental test which has been completed in the past at the same supersonic flow speed and the reader is referred to the work of Fowler [21]. An image of the filled in cavity and the broadband pressure spectra are shown in Figures 14 and 15. In Figure 15 it can be seen that no peaks are present due to the wind tunnel itself, only a constant spectra which can be considered the "background noise" of the experiment.

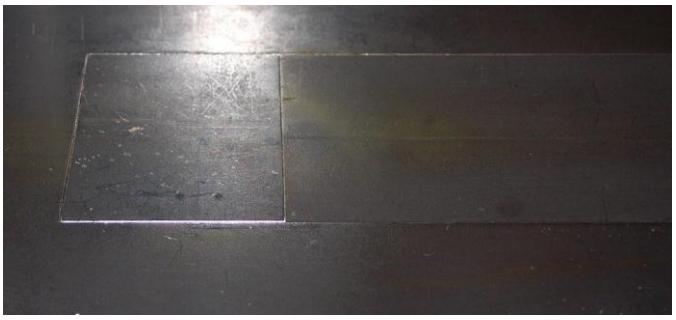

Figure 14- Clean Tunnel Photograph. (from Fowler [21])

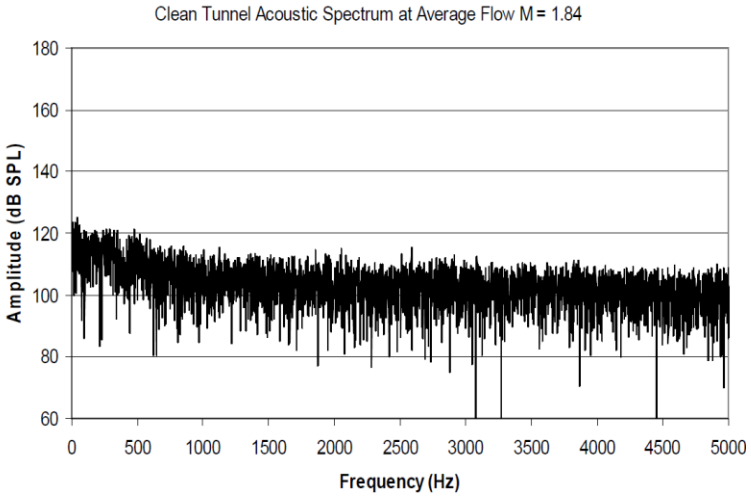

Figure 15- Clean Tunnel Acoustic Spectra. (from Fowler [21])

4.3 Configuration 1: Baseline

This first tested configuration of this study was not truly a configuration like the ones in the following sections, as it consisted of the cavity with no pins upstream (only a blank plate) as can be seen in Figure 16. The purpose of this test was to obtain a baseline, an example of how the cavity behaves with no flow control. It is only with this information that we can make any judgment on the successfulness of this flow control technique and any explanations as to what flow mechanisms caused the different pin configurations to be successful.

The data describing the sound pressure level spectrum for the baseline cavity is pictured in Figure 17. Large defined peaks in the SPL are very obviously present in the current study, especially in the second mode, just as was found by Milne [4], as can be seen in Figure 17 b). It is these peaks, as well as the overall spectra level, that we are hoping to see lowered when we look at the measurements obtained from the vertical pin configurations. This thesis aims to use PIV imaging to visualize the mechanisms of this suppression and explain both why they are present and how they cause this suppression. This will be accomplished through analyzing instantaneous velocity vector fields as well as non-dimensionalized velocity and vorticity contours.

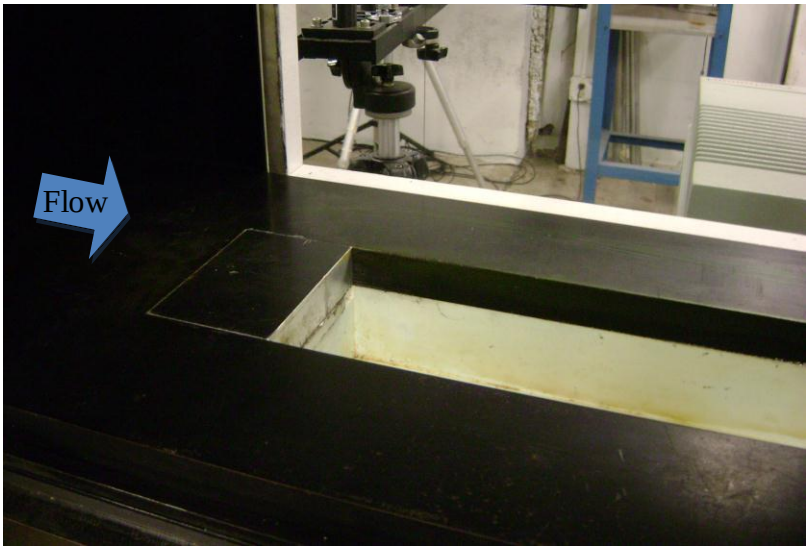

Figure 16- Baseline Blank Plate in Test Section.

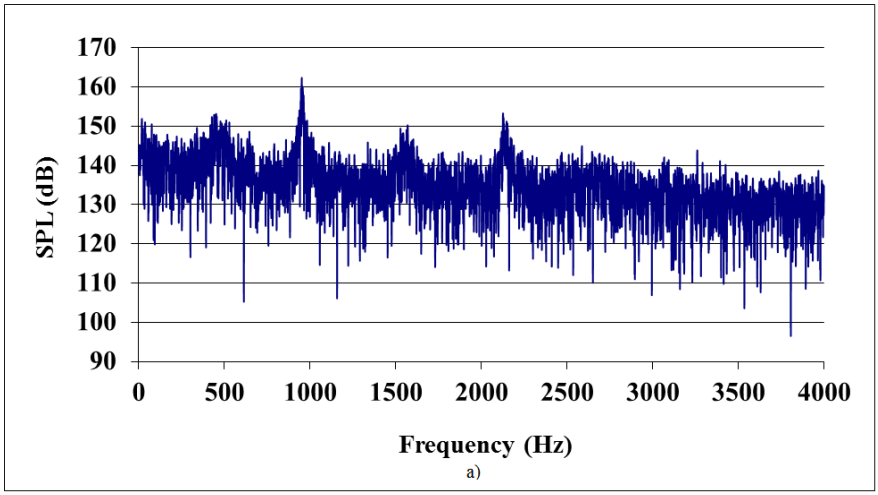

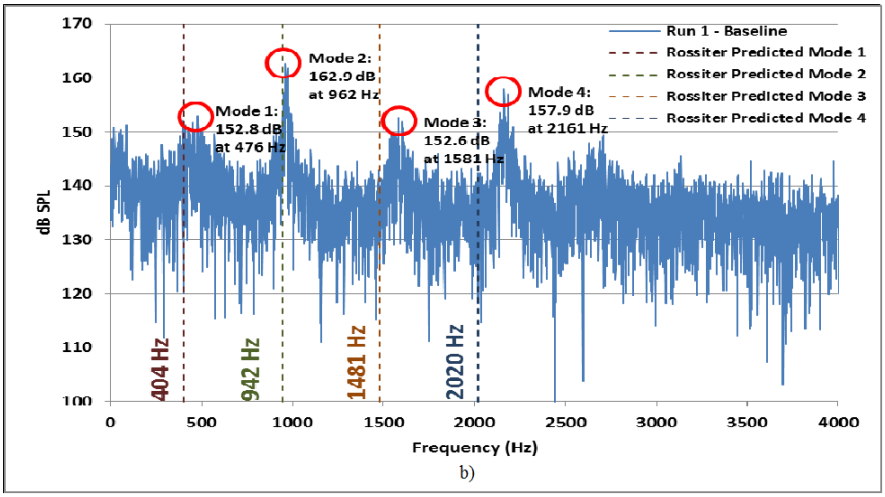

Figure 17- Baseline Cavity Acoustic Spectra from a) Current Study and b) Previous Study. (from Milne [4])

As stated before, to be able to make any assumptions about how the pin configurations are altering the flow, we must first look at the results found by testing the empty cavity. Figure 18 shows the instantaneous vector field for the baseline cavity at a single representative instance during the 120 image pairs captured. It can be seen that even after the vector validation process the incoming flow does not have a uniform profile as would be expected. This is not due to any actual inconsistencies in the freestream velocity, but instead caused by the limitations of the

current PIV setup, namely the size of the planar laser sheet which illuminates the seeding in the flow. Figure 19 from Fowler [21] shows the approximate size of the laser sheet and the field of view in which the PIV can obtain accurate results. Fowler states that the field of view is roughly 2 inches vertically and 4 inches horizontally, starting 0.5 inches before the leading edge and showing 3.5 inches of the cavity. Figure 16 seems to indicate that the actual field of view starts closer to 1 inch, corresponding to $x/L = 0.09$, before the leading edge. Either way, the front region of the vector field shown is outside the limits of reliable vectors and will therefore give erroneous values. While this region of vectors could have been excluded from all further data sets it has been left in due to the location of the front edge of the pin plate and the desire to maintain a field of view which encompasses the entire plate and all of the pins. Therefore, it must be kept in mind that the flow will not be represented accurately in this area on any further plots.

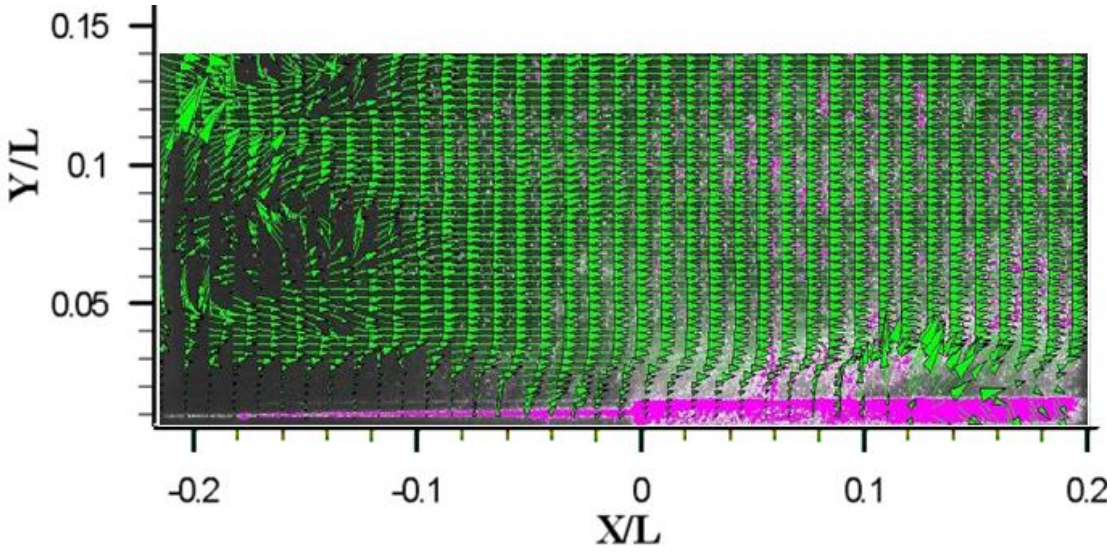

Figure 18- Baseline Cavity Instantaneous Velocity Vector Field.

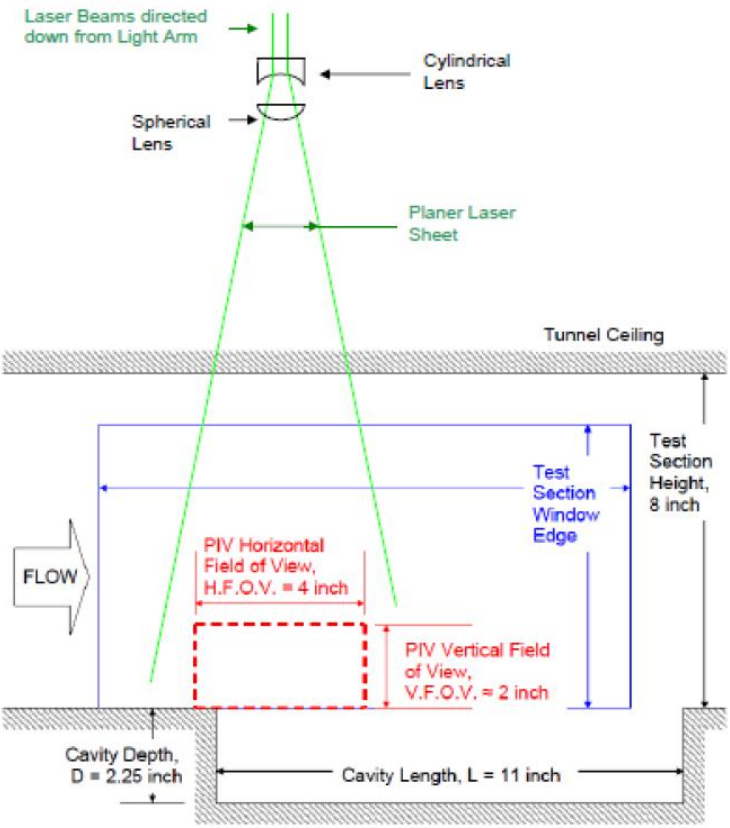

Figure 19- Sketch of PIV Setup Field of View. (from Fowler [21])

It should be noted here that a second set of tests were run using the same set of pin configurations which will be discussed here, but with a different camera field of view. This second camera position was intended for the purpose of capturing images of shear layer interactions over the cavity further downstream than was visible in the initial field of view. Due to the visual limitations of the PIV setup just presented, this data was not able to provide any useful insight into the desired region and therefore will be excluded from further discussions.

Despite the erroneous vectors due to the field of view limitations, there is still much that can be seen in Figure 18. The boundary layer along the upstream surface is visible as well as the shear layer forming at the leading edge. At the moment of this instantaneous vector field, the shear layer appears to be lifting up above the cavity. If we look at Figure 20 which is made up of a series of consecutive instantaneous velocity magnitude contours, we can see that this slight

lifting is actually part of the constant unsteadiness in the shear layer. When averaged out over the entire test (120 consecutive sets of instantaneous vector data) though, as seen in Figure 21, this unsteadiness can be seen to remain in only a very concentrated area. This region of relatively constant thickness defines the location of the boundary layer and shear layer in the flow.

In Figures 22 and 23 we can see the non-dimensional instantaneous and average contour plots for non-dimensional vorticity. This was calculated from the velocity components using a Tecplot macro. In the instantaneous contours in Figure 22, we can see the unsteady pockets of negative vorticity moving through the boundary layer and into the shear. When these instantaneous contours are averaged over the entire test, as shown in Figure 23, we can then see the very concentrated region of negative vorticity along where we know the boundary layer and the shear layer to exist. This is as would be expected, for the boundary layer is known to be a very thin region containing high gradients. Therefore very large magnitudes of vorticity would occur throughout this region, unlike in the uniform freestream flow.

Again we will make note that the apparent large amounts of vorticity in the upstream region is due to the erroneous vectors previously mentioned and not an actual characteristic of the flow.

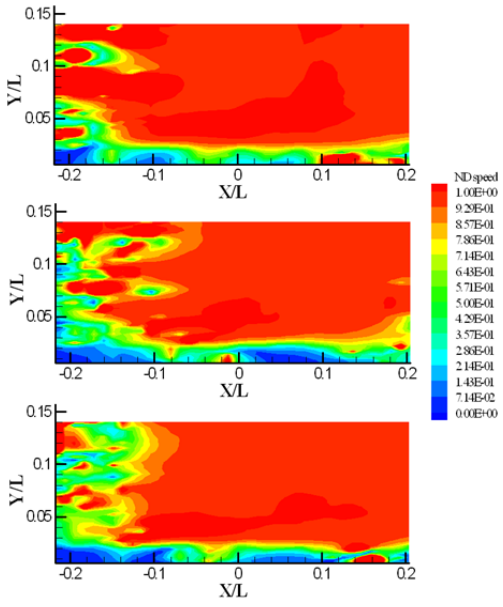

Figure 20- Baseline Non-Dimensional Instantaneous Velocity Magnitude Contours.

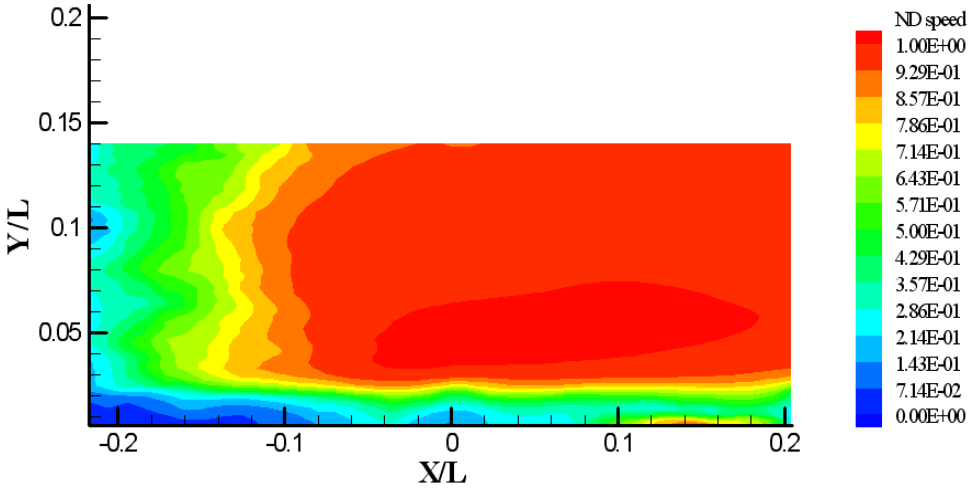

Figure 21- Baseline Non-Dimensional Average Velocity Magnitude Contour. Averaged Value Based on 120 Instantaneous Velocity Fields.

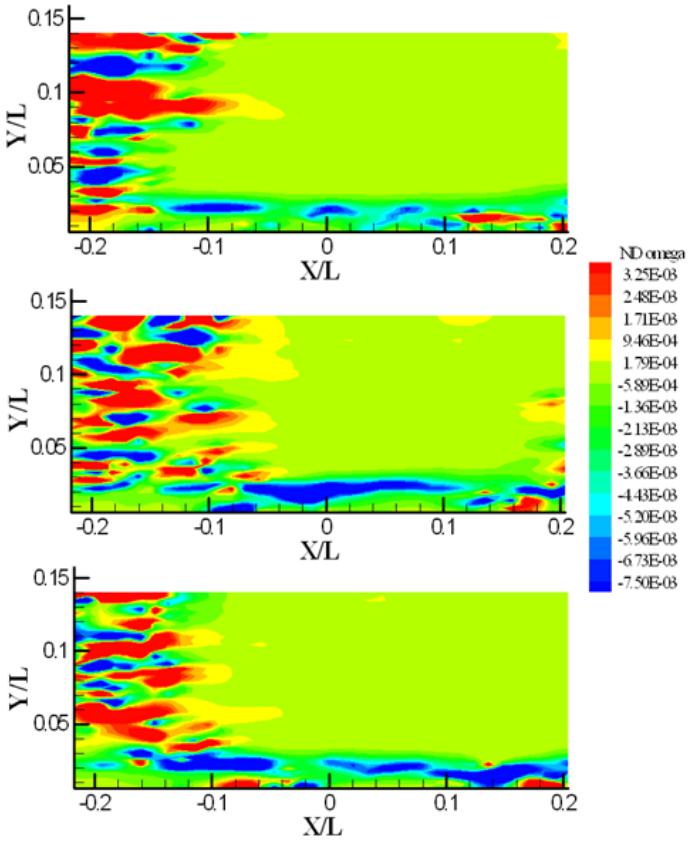

Figure 22- Baseline Non-Dimensional Instantaneous Vorticity Contours.

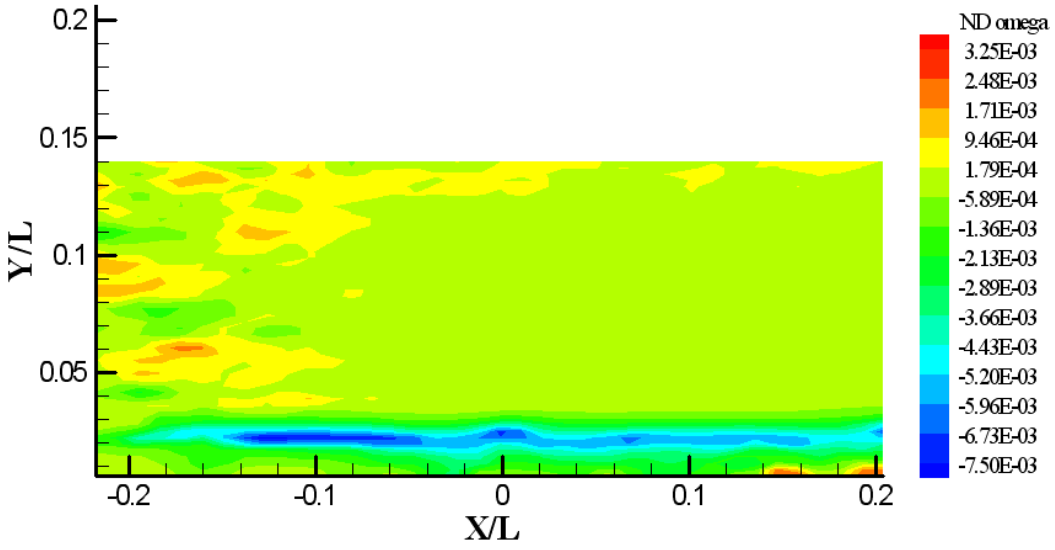

Figure 23- Baseline Non-Dimensional Average Vorticity Contour. Averaged Value Based on 120 Instantaneous Vorticity Fields.

4.4 Configuration 12: Staggered Every 2nd Row

This configuration consists of pins placed in every other hole along every second row of the pin plate. Figure 24 shows a picture of this configuration in the wind tunnel. Of the four configurations tested here, this configuration was found to have the largest amount of overall broadband spectra suppression but the lowest suppression of the second, mode. The suppression of the second mode will be focused on more than the other modes, because it is the dominant mode for this cavity setup as was seen in the baseline spectra in Figure 17. It can be seen in the acoustic spectra for this configuration, shown in Figure 25, that the second mode has been decreased by almost 20 dB compared to Figure 17 and that the peaks indicating the less dominant modes are essentially gone. Also, the overall spectra level has been decreased by more than 10 dB. These results are consistent with those obtained by Milne [4].

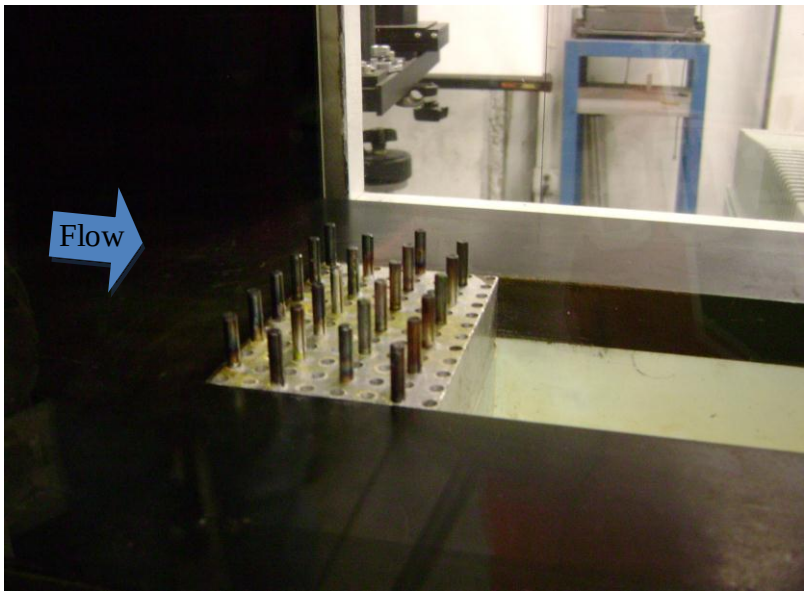

Figure 24- Configuration 12 Pin Plate in Test Section.

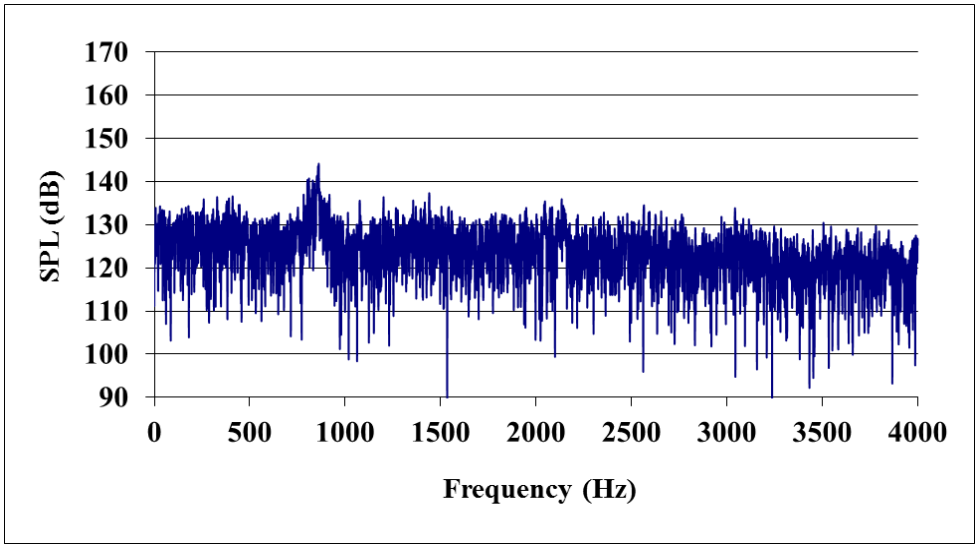

Figure 25- Configuration 12 Acoustic Spectra.

When we look at the velocity vectors, as shown in Figure 26, we can observe that the boundary layer has expanded, encompassing the pins in a low velocity region. It can also be seen that the flow is actually dipping down into the empty rows of the pin plate and therefore interacting with the individual pins and not just the configuration as a whole. The instantaneous contours in Figure 27 show this to be true as the velocity in the region of the upper pins is fluctuating instead of remaining a solid pocket of low velocity. Despite the flow having some interaction with the pins, as a whole they still form a blockage to the flow and therefore we can see a region of chaotic vectors in Figure 26 where we would expect a wake to occur. This turbulence in the flow can be seen in Figure 27 as very prominent pockets of velocity moving along the cavity length underneath the shear layer. The shear layer itself is no longer being formed at the leading edge of the cavity as it was in the baseline cavity. Instead it is formed above the cavity at the point where the flow comes off the pins. Not only is the shear layer positioned above the cavity, it also has been formed much thicker than we originally saw in the baseline. If we look at the average velocity magnitude contour in Figure 28, we can see that not only is the shear layer thicker than in the baseline when it is form, it is actually increasing in thickness as it spans over the cavity. This occurs because when the boundary layer encountered the pin configuration the characteristics of the flow were altered, and one result of this change is the thickening of the shear layer. While the exact details of the changes to the shear layer characteristics will differ based on the specific pin configurations, the general use of vertical pins in this manner will no doubt prove to be fairly consistent at obtaining some form of thickened shear layer, as we have seen here.

The flow behavior which has been noted from these figures can already be seen to be a huge difference from what it looked like in the baseline cavity, an indicator that the behavior is probably connected to the flow mechanism responsible for the acoustic suppression. If we look at the vorticity contours in Figures 29 and 30 we begin to see why the thickening of the shear layer may be causing the decrease in SPL.

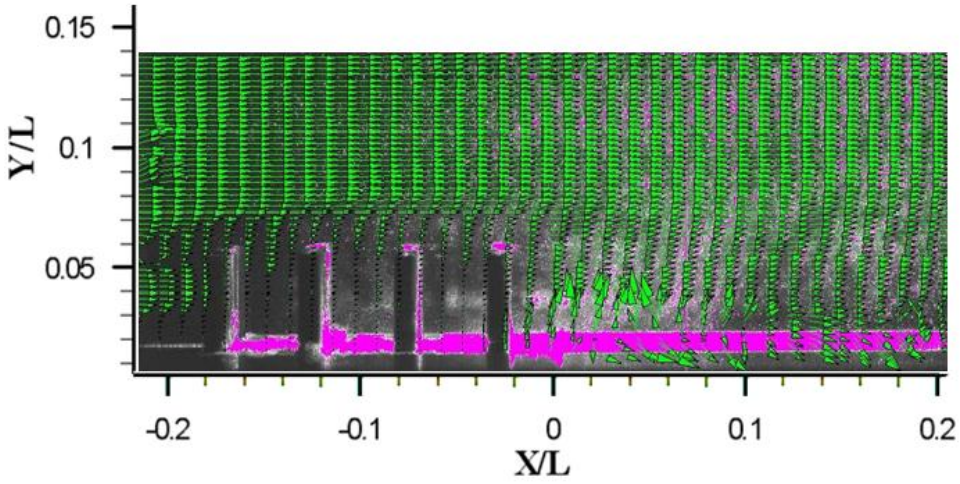

Figure 26- Configuration 12 Instantaneous Velocity Vector Field.

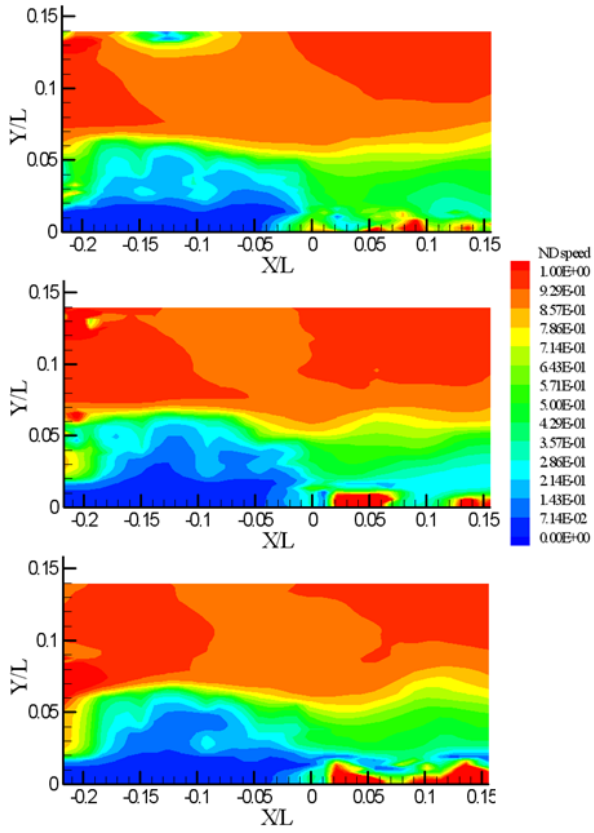

Figure 27- Configuration 12 Non-Dimensional Instantaneous Velocity Magnitude Contours.

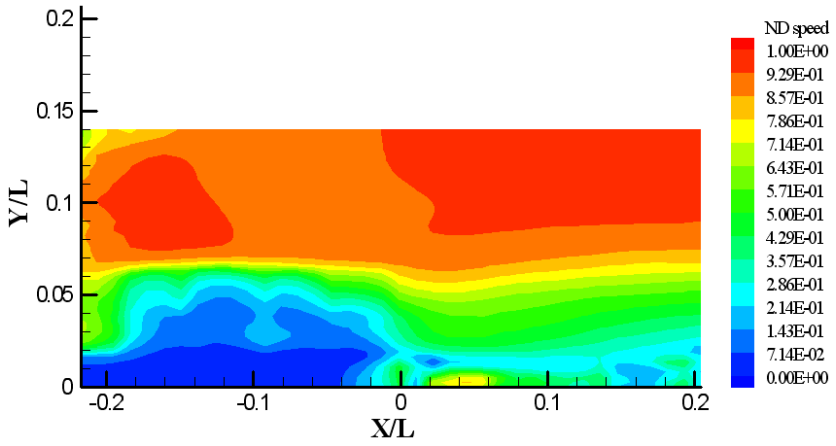

Figure 28- Configuration 12 Non-Dimensional Average Velocity Magnitude Contour. Averaged Value Based on 120 Instantaneous Velocity Fields.

In the baseline average vorticity contour we were able to clearly see a thin, concentrated region of negative vorticity inside the boundary layer and extending into the shear layer. For this configuration the average vorticity in Figure 29 isn't anywhere near as concentrated. It is still possible to see a small amount of highly negative vorticity in the portion of the boundary layer above the pins, but it isn't anywhere as strong as for the baseline case. If we look at the instantaneous contours in Figure 30 we can see the actual amount of vorticity in the flow is actually still relatively large at any given moment, but because it is concentrated in smaller pockets moving through the flow and fluctuating with time, it ultimately averages out to a smaller value which we can use to compare between configurations.

Next if we consider the shear layer, it can be noted that at this point the vorticity distribution changes. As the shear layer is expanding and growing, the vorticity is actually being diffused. This is the result of the changes to the flow characteristics due to introducing the pins to the upstream flow. This particular change in characteristics, the thickening shear layer and vorticity diffusion, are causing a suppression of the acoustic spectra which is what we had hoped to achieve with the vertical pin concept.

We can also note the presence of vortical structures below the shear layer in the cavity where we previously saw the velocity fluctuations in the wake of the pins.

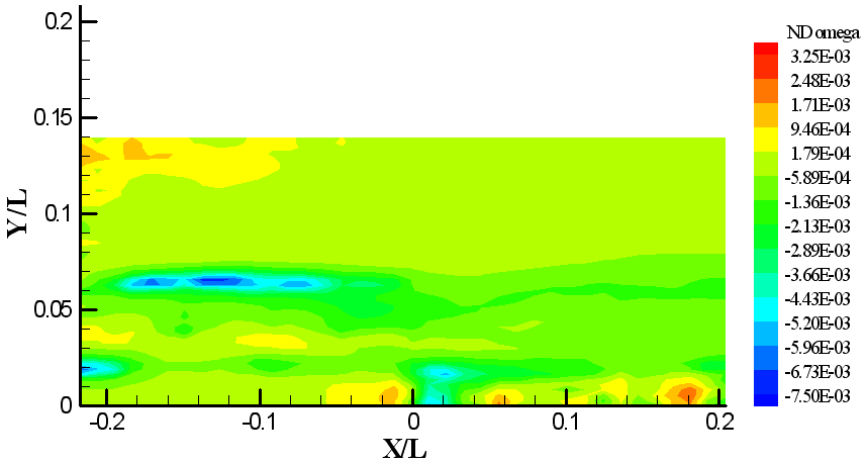

Figure 29- Configuration 12 Non-Dimensional Average Vorticity Contour. Averaged Value Based on 120 Instantaneous Vorticity Fields.

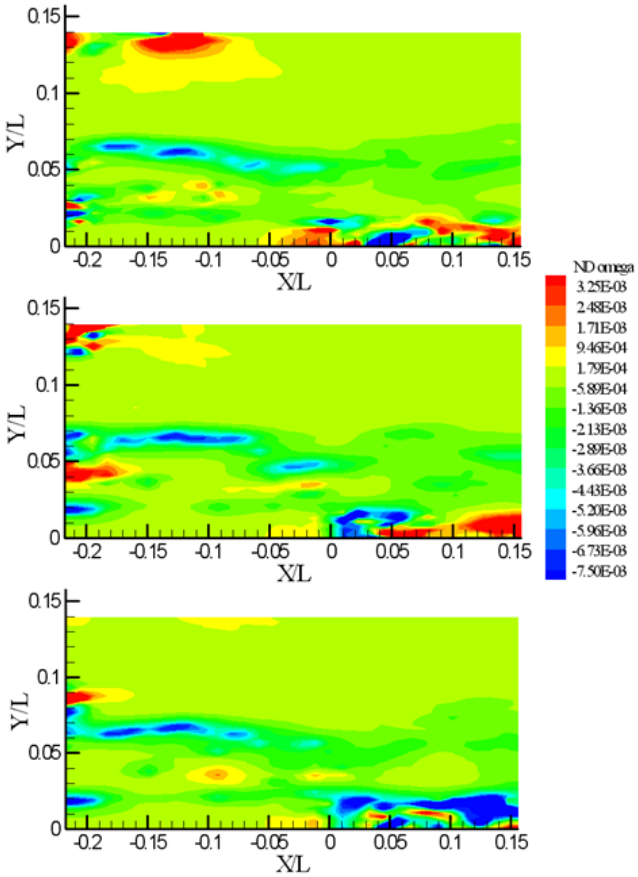

Figure 30- Configuration 12 Non-Dimensional Instantaneous Vorticity Contours.

4.5 Configuration 13: Full plate

Configuration 13, shown in Figure 31, consisted of the entire plate full of pins and therefore it was the most densely spaced configuration possible. It had the lowest overall spectra suppression of the four configurations tested here but only by roughly a decibel. It also had the second least amount of suppression in the second mode. Figure 32 shows the acoustic spectra for this configuration, and from it we can see that while the second mode was reduced by roughly 20 dB from the baseline, the other modes are still very visible and weren't suppressed as much as in configuration 12. Again, these results agree with those obtained by Milne. Any differences between the two studies fall within a few decibels which can be considered a reasonable error value for repeatability.

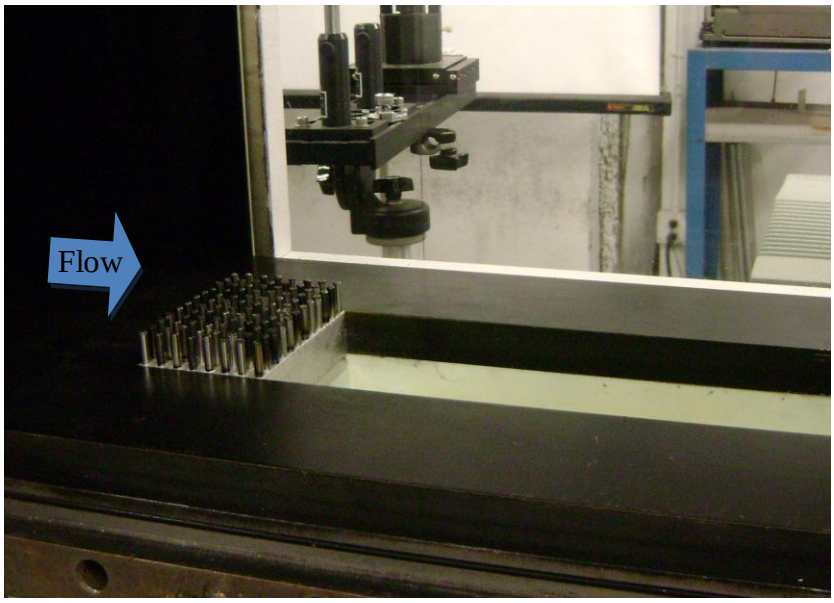

Figure 31- Configuration 13 Pin Plate in Test Section.

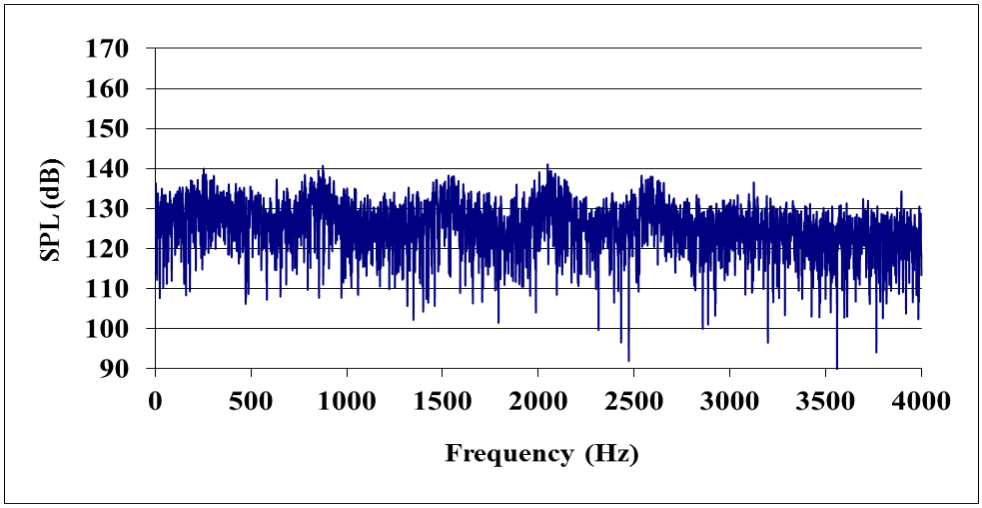

Figure 32- Configuration 13 Acoustic Spectra.

It can be seen in the vector field shown in Figure 33 that, unlike the previous configuration where there was a certain amount of flow interaction with the pins, in this configuration the flow is treating the mass of pins as much more like a solid body. Flow doesn't seem to be interacting with the individual pins much, if at all. This fact is supported by the much larger and more defined low velocity region in the average velocity contour in Figure 34. Even looking at the instantaneous contour in Figure 35, this region does not significantly change or alter with the incoming flow.

The shear layer once again forms from the expanded boundary layer off the top of the pin configuration. Again it is thicker than the shear layer formed with the baseline and increasing in thickness as it spans the cavity. This behavior is just like that seen with configuration 12 and supports the theory that this is the general altered characteristic of the shear layer for cavity flow with vertical leading edge pins. To be able to see the smaller change in flow characteristics caused by the different pin configurations, we must once again look at the vorticity contours.

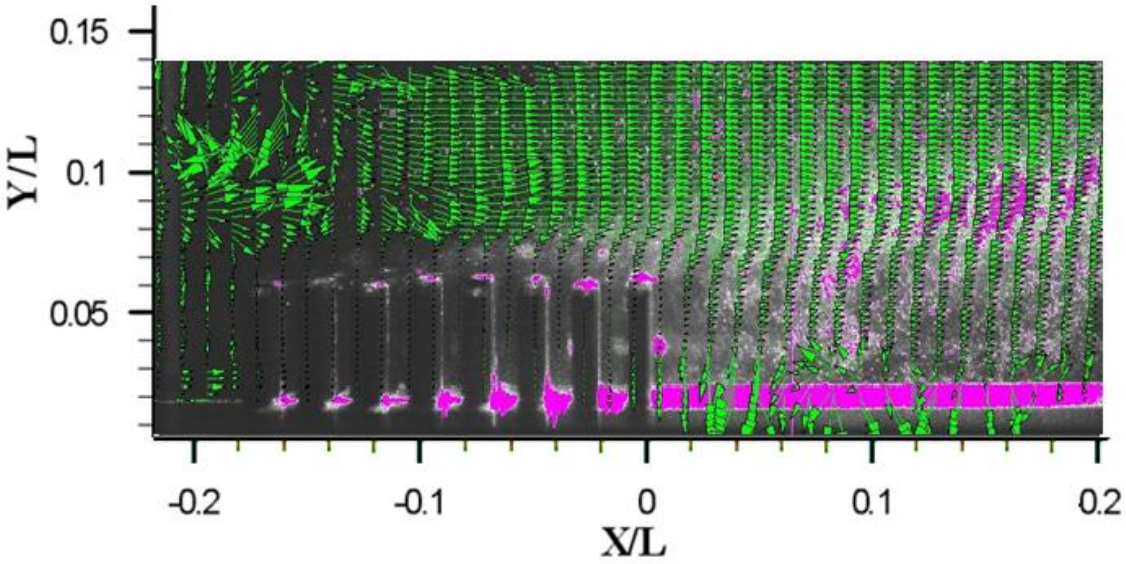

Figure 33- Configuration 13 Instantaneous Velocity Vector Field.

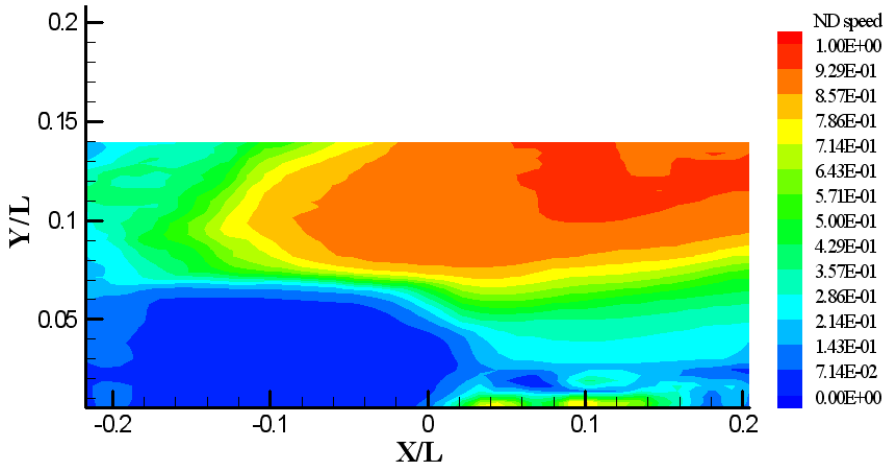

Figure 34- Configuration 13 Non-Dimensional Average Velocity Magnitude Contour. Averaged Value Based on 120 Instantaneous Velocity Fields.

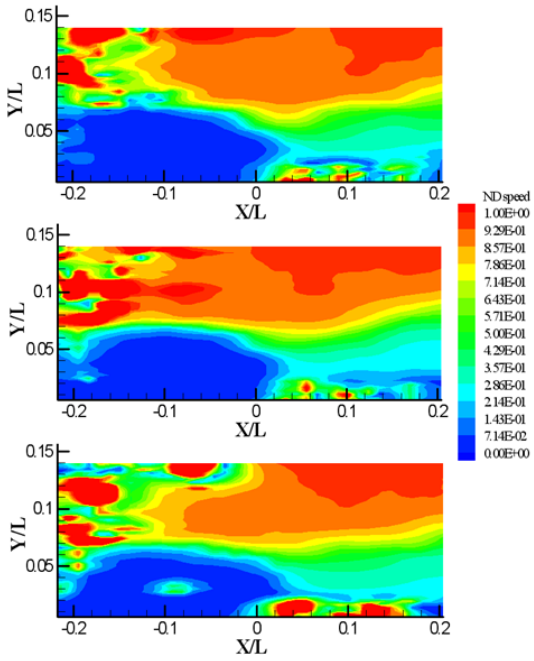

Figure 35- Configuration 13 Non-Dimensional Instantaneous Velocity Magnitude Contours.

At first glance, the average vorticity contour for this configuration looks very similar to the previous one, but several small differences are present. It is these differences which define the exact characteristics of the flow due to the specific pin configuration in use. For the full pin plate, the vorticity in the portion of the boundary layer above the pins seems to lie further forward then in the previous configuration. Also in configuration 12 the average boundary layer vorticity appeared more segmented while for this test it was a single more defined region. This is no doubt at least partially due to the lack of flow interaction with the pins as there was previously. This concentration of vorticity in the boundary layer seems to have also resulted in the shear layer being more concentrated. If we compare the velocity magnitude contours between configuration 12 and the current one, the shear layer does indeed seem to be slightly less thick for the full pin plate. This would indicate that less vorticity diffusion is occurring in the shear layer. A fact supported by Figures 36 and 37 which show a smaller and more concentrated region of negative vorticity over the cavity. This also may explain why the non-dominant modes in the spectra weren't suppressed as much as in configuration 2.

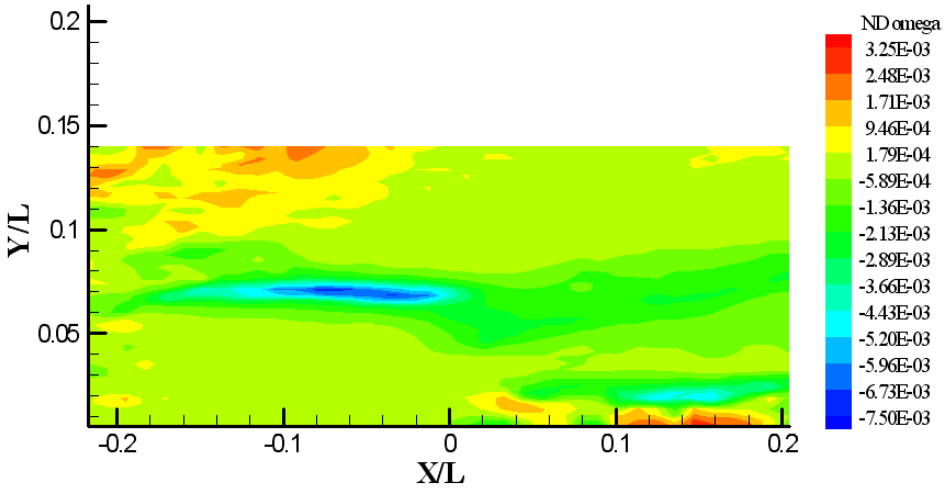

Figure 36- Configuration 13 Non-Dimensional Average Vorticity Contour. Averaged Value Based on 120 Instantaneous Vorticity Fields.

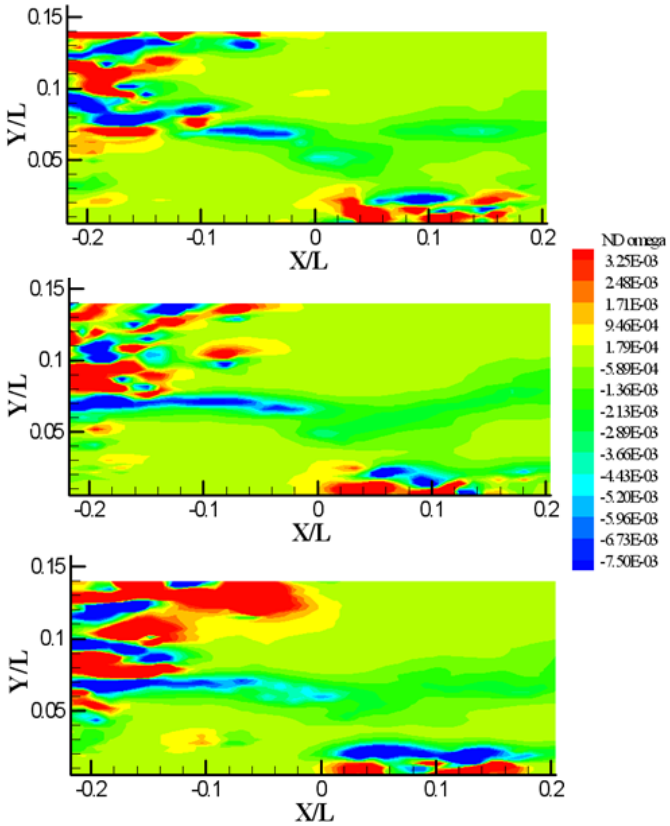

Figure 37- Configuration 13 Non-Dimensional Instantaneous Vorticity Contour Series.

4.6 Configuration 15: Every Other Row Open

In this configuration, every other row is full of pins, and the full edge of the pin plate is pointed upstream as pictured in Figure 38. The suppression obtained from this configuration was the second highest in both overall spectra reduction as well as specifically in the second mode. If we compare the acoustic spectra in Figure 39 with the previous ones we can see that the suppression of the non-dominant modes is slightly better than configuration 13, but not as good as configuration 12. And for the second mode it seems to have similar suppression to configuration 13, roughly 22 dB.

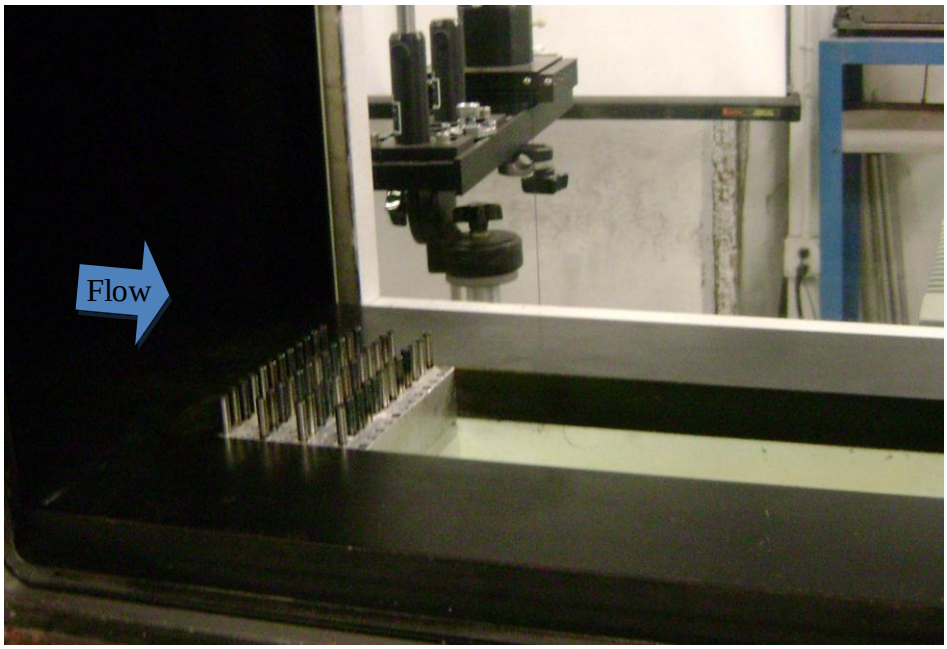

Figure 38- Configuration 15 Pin Plate in Test Section.

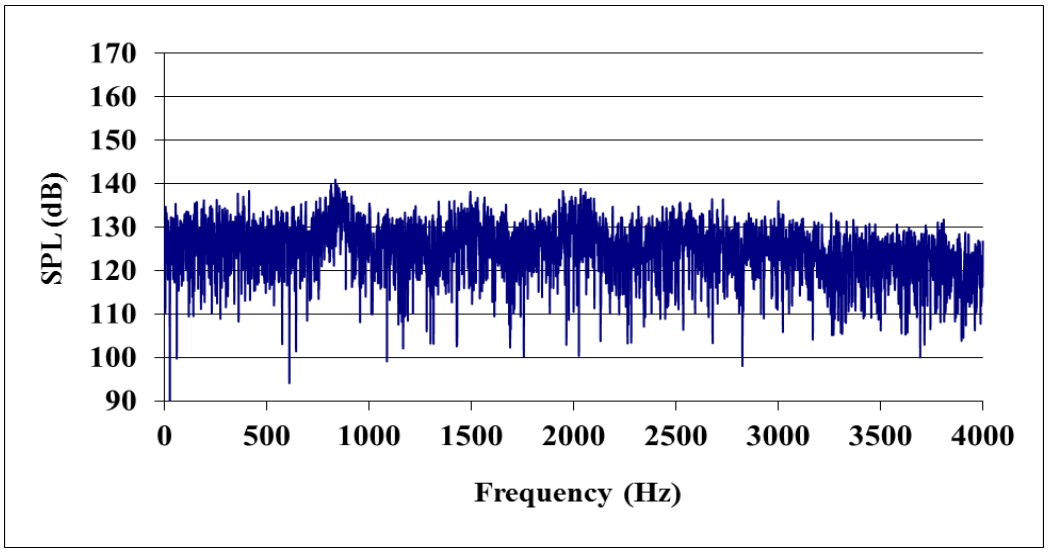

Figure 39- Configuration 15 Acoustic Spectra.

Once again, the empty rows in this configuration, similar to configuration 12, allow for the flow to interact with the pins by dipping in between the rows. As can be seen in Figures 40 through 42, the flow interacted with the pins more than for the full pin plate, but not as much as configuration 12. This may be due to the fact that, while configuration 12 also had every other row empty of pins, the pins in those rows were also staggered, while this configuration had solid rows. Therefore they wouldn't let as much flow through horizontally; any interaction would have to occur from flow dipping down from above. Disregarding the erroneous vectors at the front of the image, Figure 40 looks almost identical to Figure 26, but the slight differences become more apparent in the contour plots.

Figure 41 shows limited signs of the flow interaction which Figure 40 implied, but it is much more visible in the instantaneous contours in Figure 42. Here the very top portion of the boundary layer is fluctuating similar to that seen with configuration 12. This type of motion was not present at all in configuration 13.

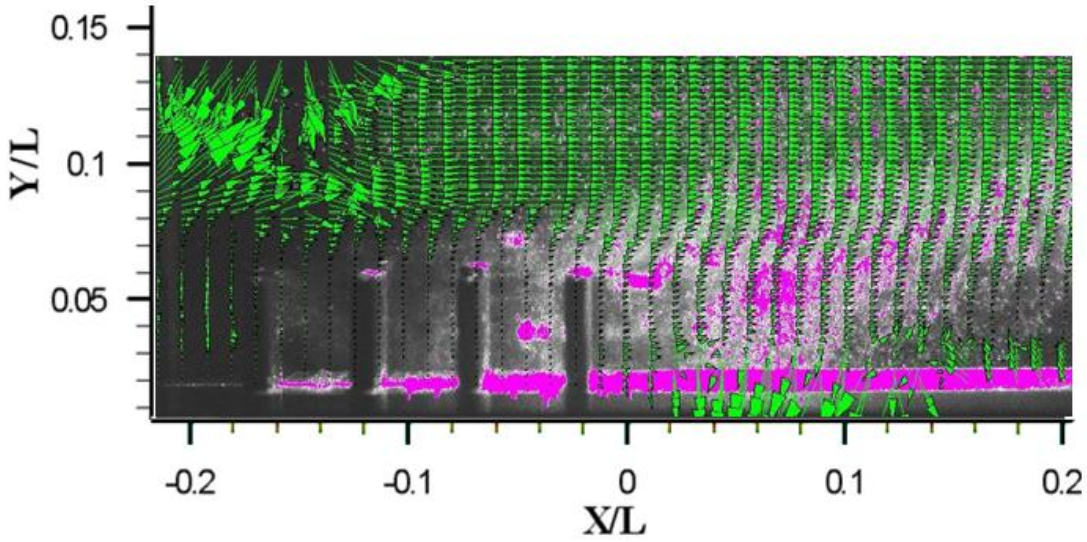

Figure 40- Configuration 15 Instantaneous Velocity Vector Field.

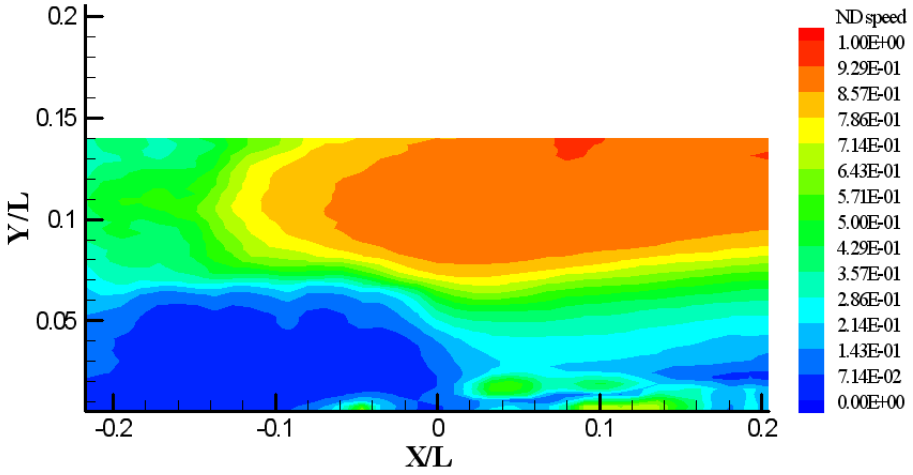

Figure 41- Configuration 15 Non-Dimensional Average Velocity Magnitude Contour. Averaged Value Based on 120 Instantaneous Velocity Fields.

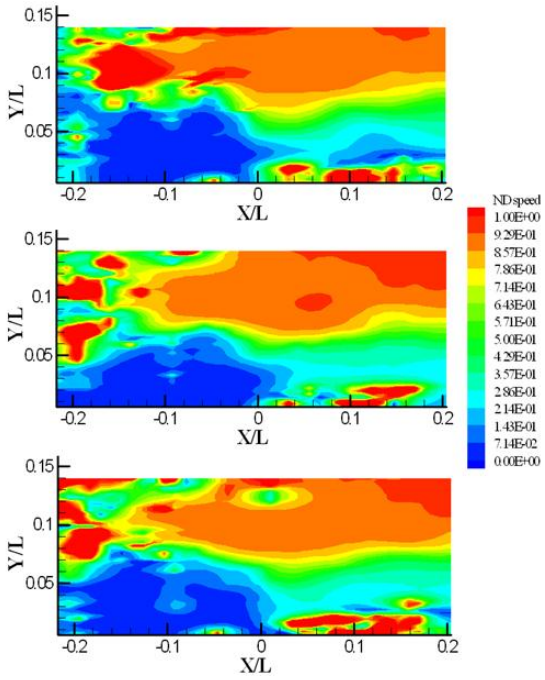

Figure 42- Configuration 15 Non-Dimensional Instantaneous Velocity Magnitude Contours.

Once again a thick shear layer is formed by the pin's interactions with the boundary layer. This thickness also once again increases as it spans the length of the cavity. These are the same set of general flow characteristics which are present in all of the configurations tested. Also, the large turbulent fluctuations which occur in the cavity in the wake of the pin plate are still visible in the contours.

When we look at the vorticity contours in Figures 43 and 44 we can see more clearly the differences between this configuration and its predecessors, as has been the case. In Figure 43, the boundary layer vorticity pocket that usually exists above the pin plate is so faint it almost isn't discernible. Even when you look at the instantaneous contours which show the actual vorticity strength and usually vary so much with time that it averages out to a smaller value, it has very weak boundary layer vorticity compared to the previous configurations. The shear layer once again shows diffusion of the vorticity as it thickens and spans the cavity, but similar to configuration 13 the diffusion doesn't seem to be as strong.

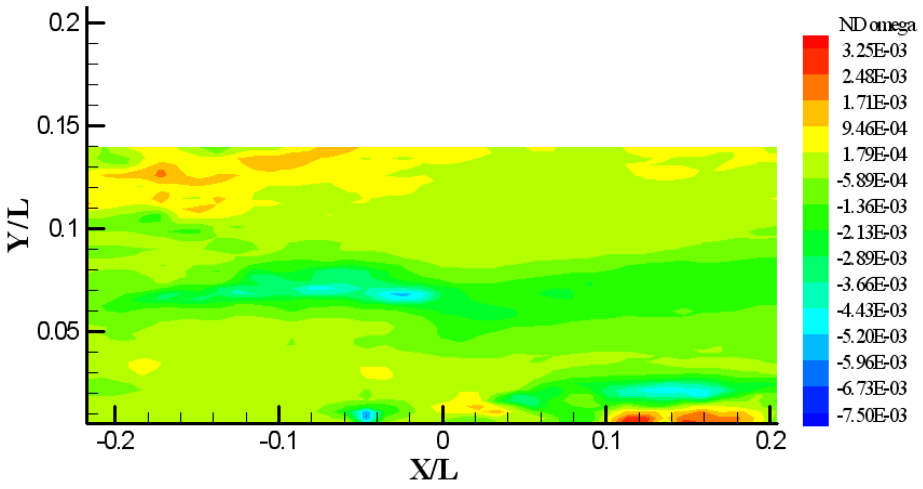

Figure 43- Configuration 15 Non-Dimensional Average Vorticity Contour. Averaged Value Based on 120 Instantaneous Vorticity Fields.

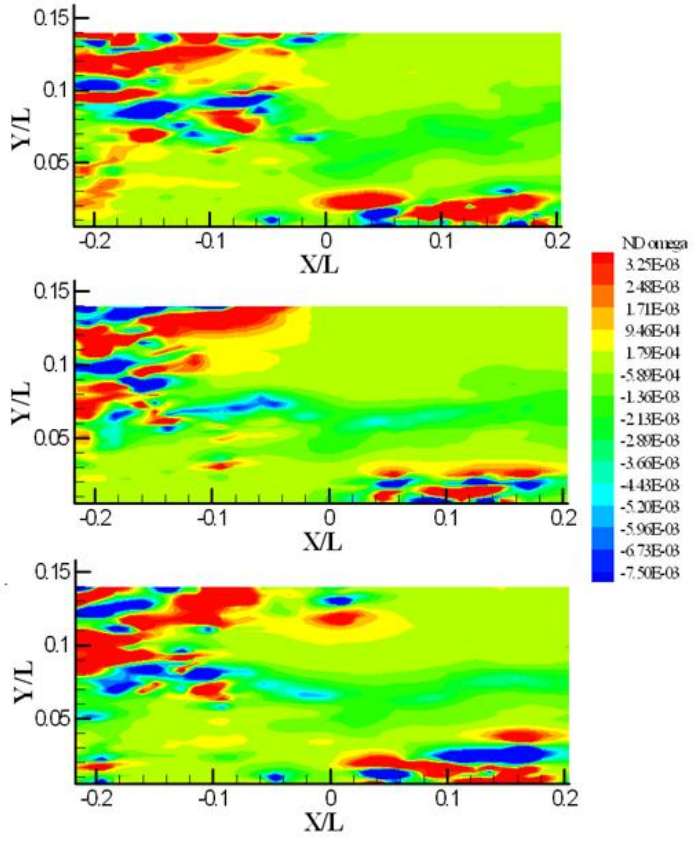

Figure 44- Configuration 15 Non-Dimensional Instantaneous Vorticity Contours.

4.7 Configuration 16: Staggered Row-to-Row

For the final configuration tested, pins were placed every other row and in a staggered pattern as can be seen in Figure 45. This configuration had the highest dominant mode suppression of all the configurations, both according to the tests by Milne [4] as well as the current study. Figure 46 shows the acoustic spectra where the large suppression of the second mode can be easily seen compared to all the previous configurations, a decreased of almost 25 dB. The overall acoustic broadband suppression was only the third highest of the configurations tested, but once again, the differences in the average broadband between tests using flow control were only one to two decibels.

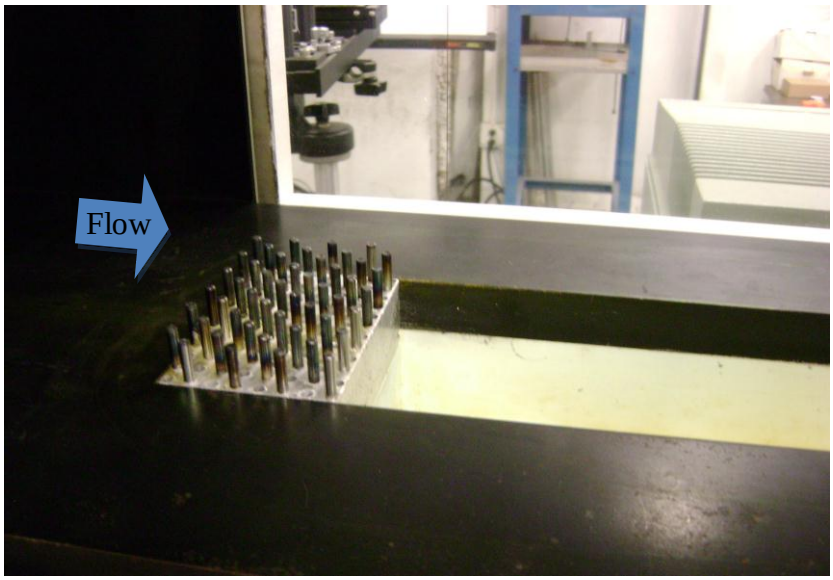

Figure 45- Configuration 16 Pin Plate in Test Section.

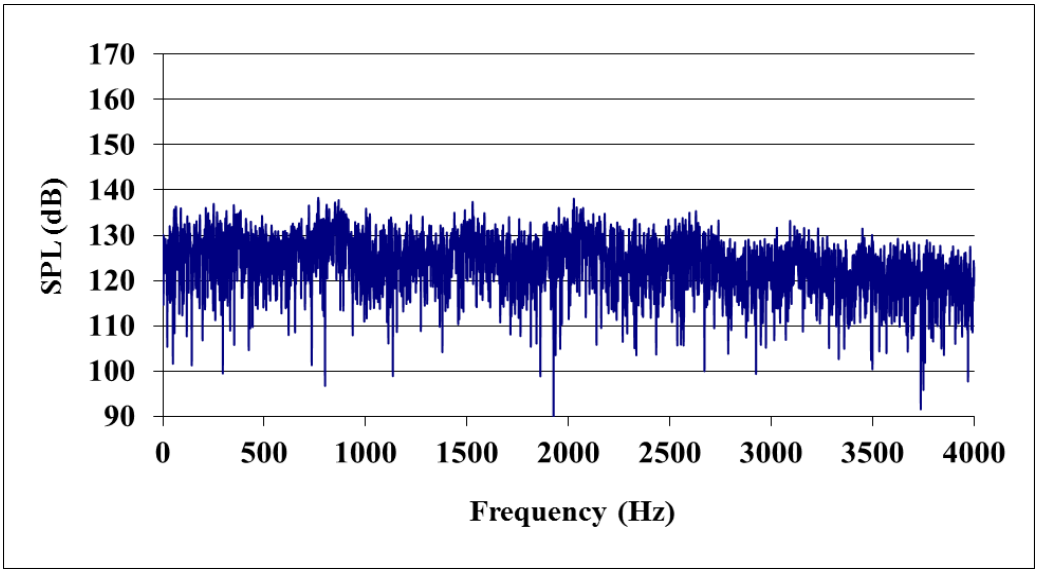

Figure 46- Configuration 16 Acoustic Spectra.

In this configuration, the pins were evenly spaced and staggered across the entire pin plate instead of leaving any empty rows. Therefore once again the flow interacted with the individual pins less and the pin plate as a whole more, as can be seen in the vector field in Figure 47. This is effect is very similar to the full pin plate configuration and the low velocity area in Figure 48 does indeed look a lot more like Figure 34 than any of the other configurations. If we look at the shear layer itself in Figure 48, while it doesn't seem to thicken as much or as quickly as usually seen on its upper surface of previous configurations, the shear layer itself is still very thick. Instead it seems to reach further down and interact more with the turbulent flow inside the cavity.

The turbulent wake flow in the cavity which can be seen in the instantaneous contour in Figure 49 is still present but doesn't seem to be as large as in previous cases. This could be related to why the shear layer is still so thick even though it doesn't expand upwards as much as other configurations.

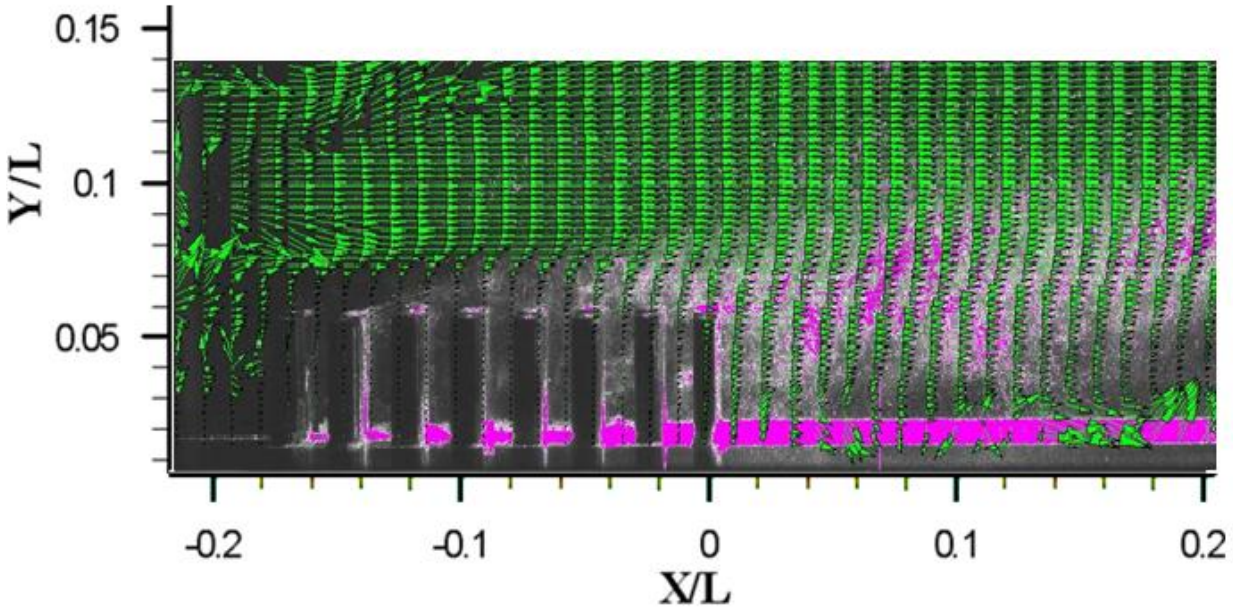

Figure 47- Configuration 16 Instantaneous Velocity Vector Field.

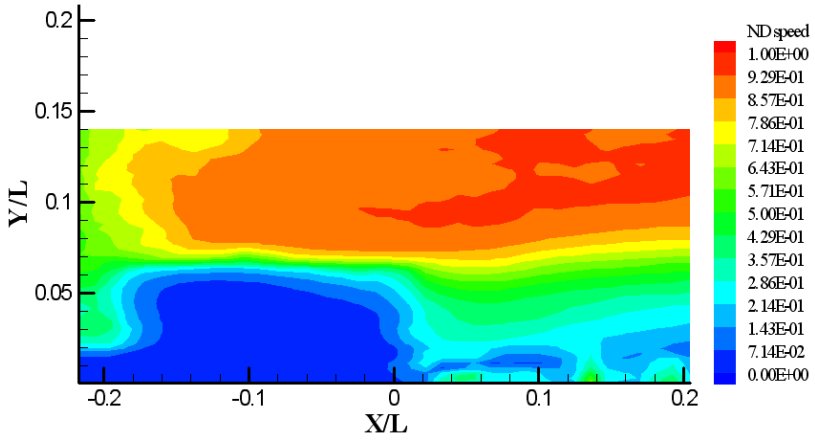

Figure 48- Configuration 16 Non-Dimensional Average Velocity Magnitude Contour. Averaged Value Based on 120 Instantaneous Velocity Fields.

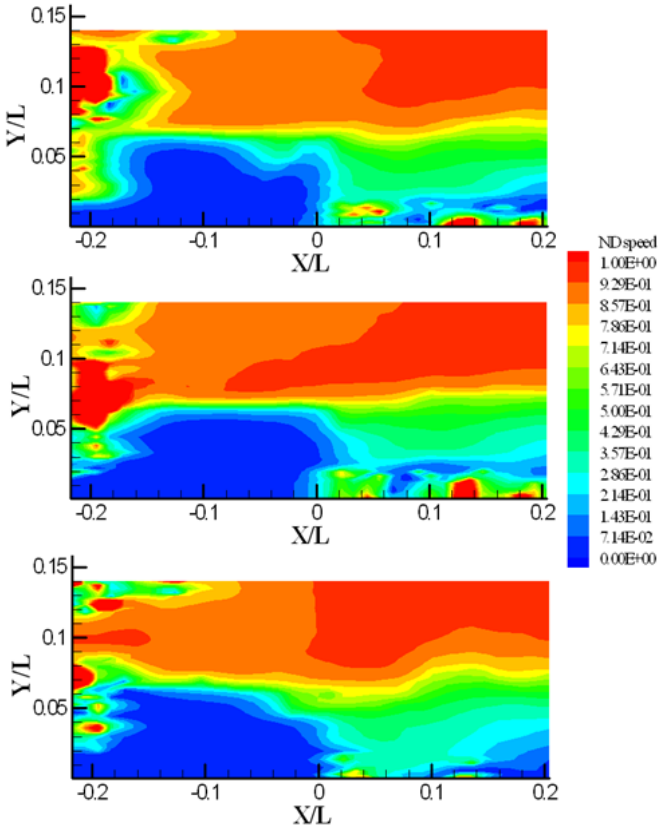

Figure 49- Configuration 16 Non-Dimensional Instantaneous Velocity Magnitude Contours.

In this final configuration, the concentrated, negative, non-dimensional vorticity zone inside the boundary layer has once again appeared above the pins as is visible in Figure 50. This region is actually more concentrated than we have seen since the baseline average vorticity contour. This is no doubt due to the fact that the strength and placement of this vorticity region doesn't seem to fluctuate over time, as can be seen in the instantaneous contours in Figure 51. Despite this, the shear layer seems to diffuse the vorticity more than the two previous configurations, but not quite as much as configuration 12. While the amount of the shear layer through which the vorticity is being diffused may not be as extensive, as can be seen in Figure 51, the large amount of vorticity in the boundary layer is still diffused more than configurations with smaller concentrations of vorticity in the boundary layer.

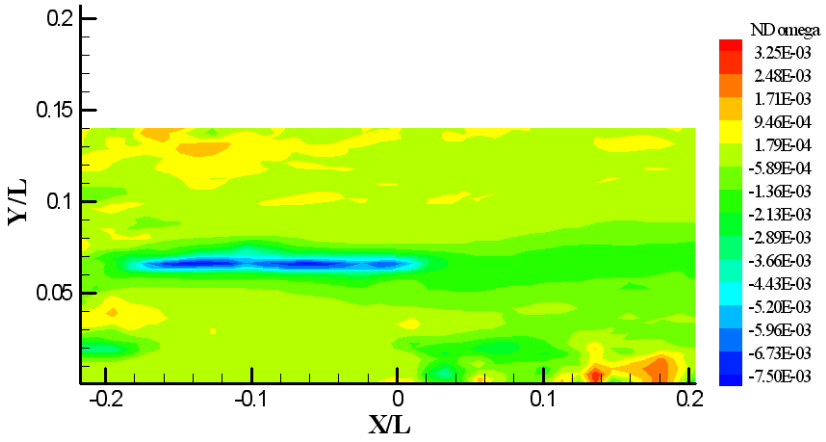

Figure 50- Configuration 16 Non-Dimensional Average Vorticity Contour. Averaged Value Based on 120 Instantaneous Vorticity Fields.

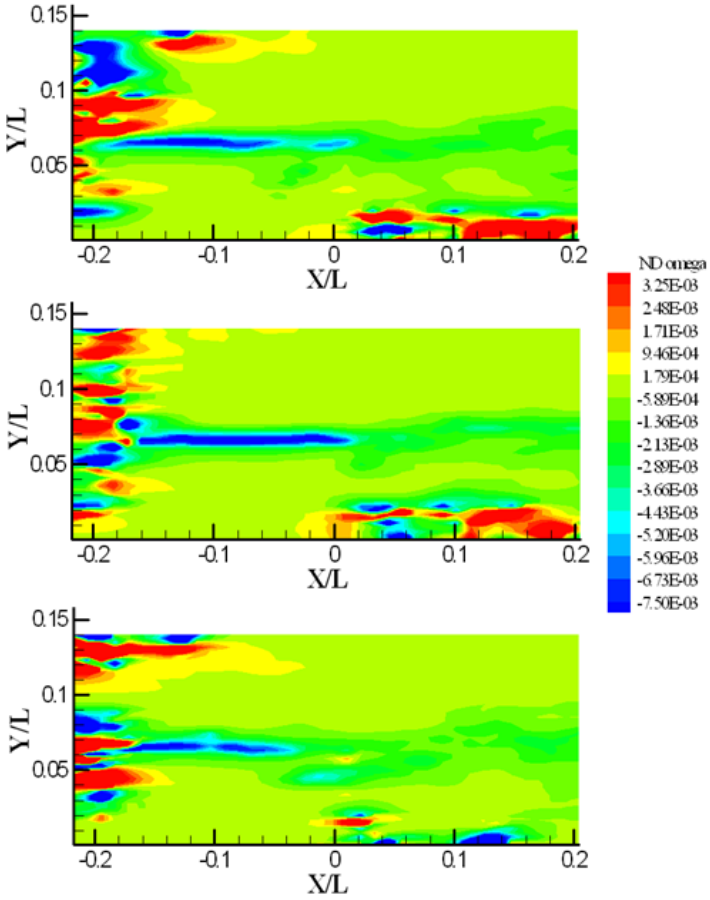

Figure 51- Configuration 16 Non-Dimensional Instantaneous Vorticity Contours.

4.8 Configurations Summarized

Based on the observations made from the results of these tests, we can summarize what the PIV flow visualization has shown us about the suppression mechanism involved in the flow control technique. By comparing the acoustic spectrum, vector field and velocity and vorticity contours of the different configurations with the baseline, some patterns became apparent.

It was determined that vertical pins placed upstream of a cavity leading edge interact with the boundary layer and alter the characteristics of the flow. This interaction is brought about through the flow mechanics created by the boundary layer passing by the cylindrical bodies of the pins. Circular cylinders have been studied extensively to understand the exact flow properties which are created due to their presence. One such study is that done by Kawamura, Hiwada, Hibrino, Mubuchi, and Kumada [31] looking at flow past a finite cylinder on a flat plate. Bluff body flow, such as that described by Kawamura, et al. and as can be seen in Figure 52, creates vorticies off each cylindrical pin which then interact with the pins further downstream. It is the interaction of these vortices which creates the alterations in the characteristics of the boundary layer flow. These characteristics are then transferred to the shear layer where we see the effects of these changes more clearly. The general effect of using vertical pin configurations is the change in the vorticity distribution in the shear layer. The most obvious effect that this generates is the formation of a much thicker shear layer than the one in the baseline cavity. This thicker shear layer also tends to increase in thickness as it spans the cavity. These are the general effects observed to be true for vertical pin cavity flow control.

For various pin configurations, the pattern of vorticies shed from the cylindrical pins creates differences in boundary layer and thereby the shear layer. The effects which occur due to these unique flow patterns from each of the specific formation of pins can be observed by looking specifically at the vorticity contours. Here we can see the details of how the vorticity is being distributed and diffused.

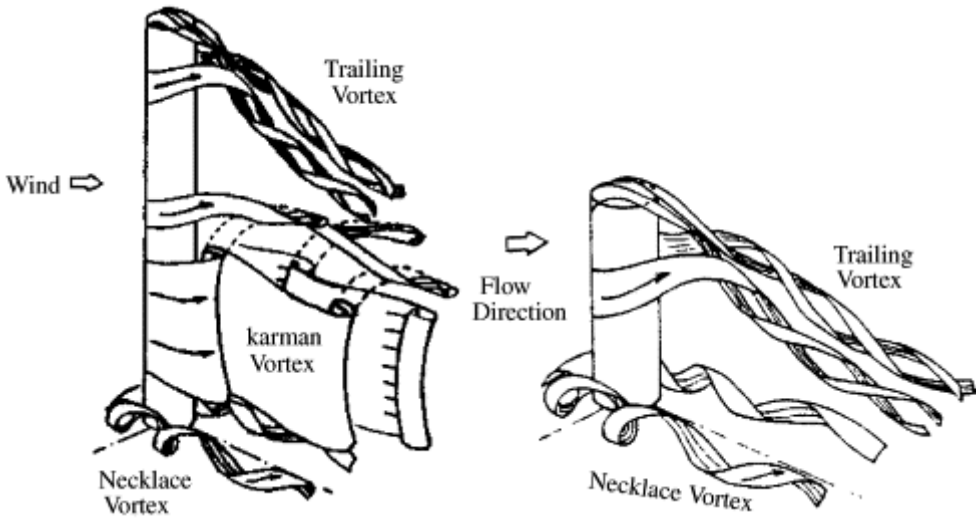

Figure 52- Vortex Shedding Off Circular Cylinders (from Kawamura, Hiwada, Hibrino, Mubuchi, and Kumada [31])

It was observed for configurations which had pins placed in a staggered pattern instead of in full lines, such as configuration 12 and 16, that the boundary layer vorticity was diffused more effectively. This ultimately seemed to result in a larger suppression of the broadband acoustic spectra versus specifically in the dominant mode. This can be seen in Figure 53.

The role vorticity distribution and diffusion plays in suppressing the dominant mode are still unclear based on the tests done in this study. Further configurations looking into the role of the boundary layer interacting with various pin configurations densities are recommended as well as choosing a more advantageous PIV setup to allow for more accurate data collection.

The values of SPL obtained in this experiment were compared to those obtained by Milne [4] and shown in Figures 53 and 54. Any slight differences between the two studies fall within a few decibels which can be considered a reasonable error value for experimental repeatability.

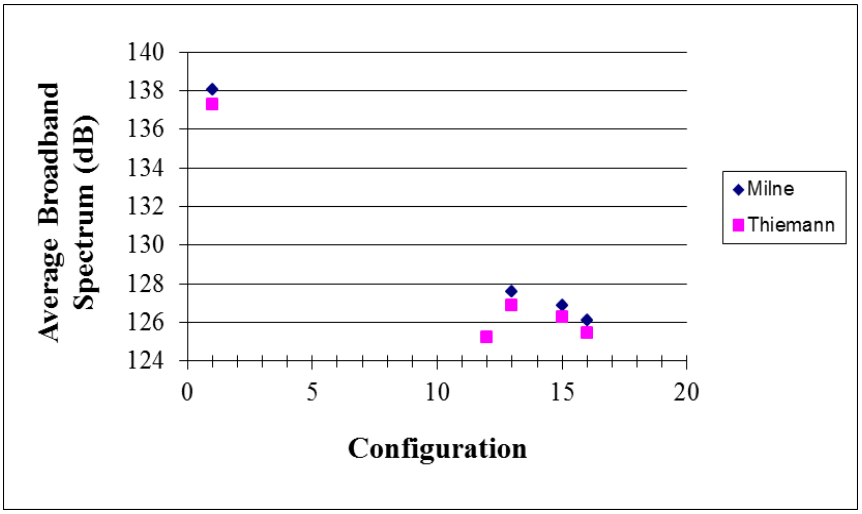

Figure 53- Compared Average Acoustic Spectrum for Configurations.

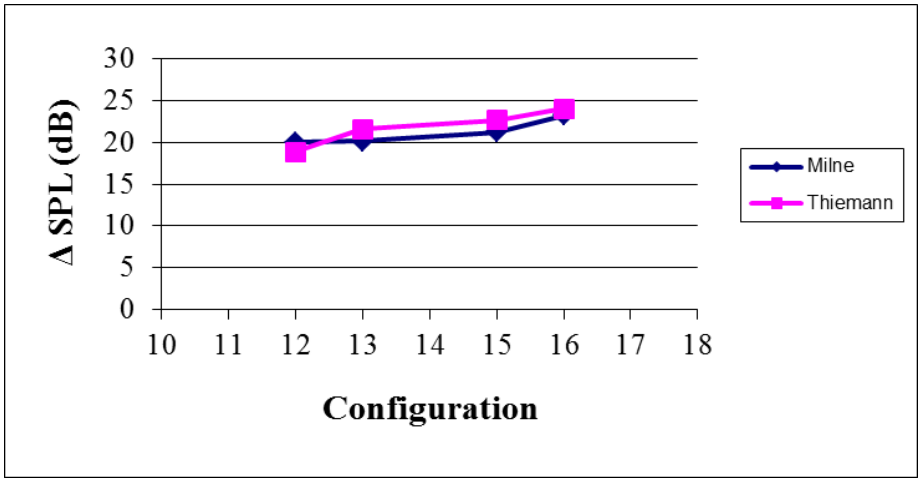

Figure 54- Compared Change in SPL for Configurations Tested.

CHAPTER 5- CONCLUSIONS AND RECOMMENDATIONS

Particle Image Velocimetry, a non-intrusive quantitative flow measurement system was employed to study the velocity and vorticity fields of an open cavity shear layer with L/D of 4.89 at Mach 1.84 with and without passive flow control implementations. The purpose of this study was to attempt to understand and explain flow mechanisms behind acoustic suppressions which are obtained using different leading edge, vertical pin configurations. Each pin configuration varied the number and placement of pins while pin height remained a constant ½ inch. The four configurations chosen to be studied were based on the best acoustic suppression results obtained by Milne [4]. The study looked at the acoustic spectrum, velocity vector field data, as well as the changes in the velocity and vorticity fields, created by each pin configuration to determine and understand the physical mechanism and source of attenuation of this type of cavity flow control technique.

The following conclusions were reached:

1. Altering the characteristics of the boundary layer causes a redistribution of the velocity and diffusion of the vorticity in the boundary layer approaching the cavity and hence the cavity shear layer.

2. Vertical pin configurations at the leading edge of the cavity resulted in flow characteristics which bring about a thickening of the shear layer which diffuses the boundary layer vorticity.

3. The boundary layer interactions with certain pin configurations vary in the degrees of redistribution of the velocity and vorticity, increasing the shear layer's ability to diffuse the boundary layer vorticity.

4. Configurations using a staggered pattern generated vorticity diffusion in the shear layer more effectively, which lowered the peaks and the broadband overall acoustic spectrum.

5.2 Recommendations

Further testing should look specifically into the shear layer over the cavity. The current PIV laser and optical setup would have to be adapted to accommodate this step.

Based on the results found in this study a series of new configurations are recommended to investigate the possible flow mechanisms which bring about suppression in the dominant mode, as well as looking further into the proposed cause of the decreased broadband spectra. Using the same format as that used by Milne [4], these configurations are indicated in Table A.3 in the Appendix. The configurations include leaving every second row open as well as staggering pin heights to encourage the flow to interact with the pins while still providing a dense configuration.

LIST OF REFERENCES

[1] Heller, H.H. and Bliss, D.B., "The Physical Mechanism of Flow-Induced Pressure Fluctuations in Cavities and Concepts for their Suppression," AIAA Paper 75-491, 1975.

[2] Rockwell, D. and Naudascher, E. "Review – Self-Sustaining Oscillations of Flow Past Cavities," Journal of Fluid Engineering, Vol. 100, No. 2, pp. 152-155, 1978.

[3] Plentovich, E.B., Stallings Jr., R.L., and Tracy, M.B., "Experimental Cavity Pressure Measurements at Subsonic and Transonic Speeds," NASA TP-3358, 1993.

[4] Milne, G.J., "An Experimental Investigation of Supersonic Cavity Flow Control Using Upstream Cylindrical Rods," UTSI Report 12/17, University of Tennessee Space Institute, Tullahoma, TN, Aug. 2012.

[5] Karamcheti, K., "Acoustic Radiation from Two-Dimensional Rectangular Cutouts in Aerodynamic Surfaces," NACA TN-3478, 1955.

[6] Roshko, A., "Some Measurements of Flow in a Rectangular Cutout," NACA TN-3488, 1955.

[7] Rossiter, J.E., "Wind Tunnel Experiments on the Flow over Rectangular Cavities at Subsonic and Transonic Speeds," Aeronautical Research Council R&M No. 3438, 1966.

[8] Heller, H.H., Holmes, D.G., and Covert, E.E., "Flow-Induced Pressure Oscillations in Shallow Cavities," Journal of Sound and Vibration, Vol. 18, No. 4, pp. 545-553, 1971.

[9] Tam, C.K.W., and Block, P.J.W., "On the Tones and Pressure Oscillations Induced by Flow Over Rectangular Cavities," Journal of Fluid Mechanics, Vol. 89, Part 2, pp. 373-399, 1978.

[10] Seiner, J.M., Jansen, B.J., and Murray, N.E., "Weapons Bay Acoustic Suppression at Mach 2," AIAA 2008-60, 2008.

[11] Ukeiley, L., Sheehan, M., Coiffet, F., Alvi, F., Arunajatesan, S., and Jansen, B., "Control of Pressure Loads in Geometrically Complex Cavities, " Journal of Aircraft, Vol. 45, No. 3, pp. 1014-1024, 2008.

[12] Ukeiley, L., and Murray, N., "Velocity and Surface Pressure Measurements in an Open Cavity," Experiments in Fluids, Vol. 38, No. 5, pp. 656-671, 2005.

[13] Arunajatesan, S., Kannepalli, C., Sinha, N., Sheehan, M., Alvi, F., Shumway, G., and Ukeiley, L., "Suppression of Cavity Loads Using Leading-Edge Blowing," AIAA Journal Vol. 47, No. 5, pp. 1132-1144, 2009.

[14] Cattafesta III, L.N., Williams, D.R., Rowley, C.W., and Alvi, F.S., "Review of Active Control Flow-Induced Cavity Resonance," AIAA 2003-3567, 2003.

[15] Franke, M.E., and Carr, D.L., "Effect of Geometry on Open Cavity Flow-Induced Pressure Oscillations," AIAA 75-492, 1975.

[16] Wiltse, J.M., and Glezer, A., "Direct excitation of small-scale motions in free shear flows," Physics of Fluids, Vol. 10, No. 8, pp. 2026-2036, 1998.

[17] Stanek, M.J., Sinha, N., Seiner, J.M., Pearce, B., and Jones, M.I., "High Frequency Flow Control - Suppression of Aero-Optics in Tactical Directed Energy Beam Propagation & The Birth of a New Model (Part I)," AIAA 2002-2272, 2002.

[18] Stanek, M.J., Raman, G., Ross, J.A., Odedra, J., Peto, J., Alvi, F., and Kibens, V., "High Frequency Acoustic Suppression - The Role of Mass Flow, The Notion of Superposition, and The Role of Inviscid Instability – A New Model (Part II)," AIAA 2002-2404, 2002.

[19] Stanek, M.J., Ross, J.A., Odedra, J., and Peto, J., "High Frequency Acoustic Suppression - The Mystery of the Rod-in-Crossflow Revealed," AIAA 2003-7, 2003.

[20] Loewen, R.D., "Analysis of Cavity Flow and the Effects of a Rod in Crossflow," M.Sc. Thesis, University of Tennessee, Knoxville, TN, Dec. 2008.

[21] Fowler, W.L., "Analysis and Comparison of Effects of an Airfoil or a Rod on Supersonic Cavity Flow," M.Sc. Thesis, University of Tennessee, Knoxville, TN, Dec. 2010.

[22] Fernandez, F.L., and Zukoski, E.E., "Experiments in Supersonic Turbulent Flow with Large Distributed Surface Injection," AIAA 68-129, 1968.

[23] Sarohia, V., and Massier, P.R., "Control of Cavity Noise," Journal of Aircraft, Vol. 14, No. 9, pp. 833-837, 1977.

[24] Wilcox Jr., F.J., "Experimental Investigation of Porous-Floor Effects on Cavity Flow Fields at Supersonic Speeds," NASA TP-3032, 1990.

[25] Franke, M., and Sarno, R., "Suppression of Flow-Induced Pressure Oscillations in Cavities," AIAA 90-4018, 1990.

[26] Vakili, A.D., and Gauthier, C., "Control of Cavity Flow by Upstream Mass-Injection," Journal of Aircraft, Vol. 31, No. 1, pp. 169-174, 1994.

[27] Meganathan, A.J., "An Experimental Study of Low Speed Open Cavity Flows," M.Sc. Thesis, University of Tennessee, Knoxville, TN, Dec. 2000.

[28] Radhakrishnan, S., "An Experimental and Numerical Study of Open Cavity Flows," Ph.D. Dissertation, University of Tennessee, Knoxville, TN, May 2002.

[29] Meganathan, A.J., "Adaptive Control of Axisymmetric Jets by Cavities," Ph.D. Dissertation, University of Tennessee, Knoxville, TN, May. 2005.

[30] Adrian, R.J., "Dynamic Ranges of Velocity and Spatial Resolution of Particle Image Velocimetry," Measurements Science & Technology, Vol. 8, No. 12, pp. 1393-1398, 1997.

[31] Kawamura, T., Hiwada, M., Hibrino, T., Mubuchi, I., and Kumada, M., "Flow Around a Circular Cylinder on a Flat Plate," Bulletin of JSME, Vol. 27, No. 232, pp. 2142- 2151, Oct. 1984

APPENDIX

Table A.1- HSWT Flow parameters.

Parameter	Symbol [units]	Calculated Value	Equation
Stagnation pressure	P_0 [psia]	27.94	Known (Stilling Chamber)
Static pressure	P [psia]	4.58	Known (Test Section)
Stagnation temperature	T_0 [R]	470.39	Known (Stilling Chamber)
Mach number	M	1.84	$M = \sqrt{\left(\frac{2}{\gamma - 1}\right)\left[\left(\frac{P_0}{P}\right)^{\frac{\gamma-1}{\gamma}} - 1\right]}$
Static temperature	T [R]	280.48	$T = \frac{T_0}{\left[1 + \left(\frac{\gamma - 1}{2}\right)M^2\right]}$
Local speed of sound	a [ft/s]	820.98	$a = \sqrt{\gamma RT}$
Freestream velocity	U_∞ [ft/s]	1510.61	$U_\infty = Ma$
Reynolds number	Re [/ft]	9.89×10^6	$\mathrm{Re} = \frac{\rho U_\infty L}{\mu}$

Constants (for air):

$\gamma = 1.4$; $R = 1716.49\left[\frac{\text{lbf-ft}}{\text{slug-R}}\right]$; $\rho = 2.37 \times 10^3$ slug/ft^3; $\mu = 3.62 \times 10^{-7}$ $\frac{\text{lbf-s}}{\text{ft}^2}$

Table A.2- PIV Components.

Equipment	Model #	Comments
Continuum SureLite Nd:YAG	Y200-C	532 nm Wavelength (Green Light), 200 mJ/Pulse
Articulating Laser Light Arm	610015	-
PIVCAM 10-30 CCD camera	630046	28mm F/2.8 Nikkor Lens, capable of 30 frames/sec
Synchronizer	610032	-
INSIGHT^{TM} PIV Software,	Version 3.2	-

Table A.3- Recommended Configurations.

Run Name and Number	Description	Configuration
Key	Empty Hole; 1/8" pin; 1/4" pin; 3/8" pin; 1/2" pin	FLOW
Alternate Row ½" and ¼"	Alternating rows of ½" pins followed by ¼" pins.	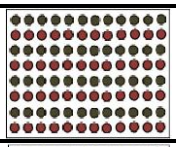
Alternate Row ½" and ⅜"	Alternating rows of ½" pins followed by ⅜" pins.	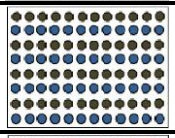
Alternate Row ½" and ¼" Staggered	Staggered alternating rows of ½" pins followed by ¼" pins.	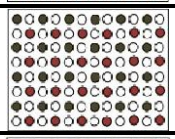
Alternate Row ½" and ⅜" Staggered	Staggered alternating rows of ½" pins followed by ⅜" pins.	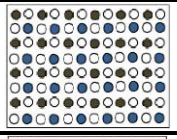
Alternate Row ½" and ¼" Staggered, Every 3rd Row Empty	Staggered alternating rows of ½" pins followed by ¼" pins with every third row entirely empty.	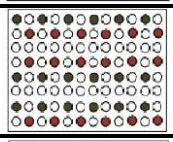
Alternate Row ½" and ⅜" Staggered, Every 3rd Row empty	Staggered alternating rows of ½" pins followed by ⅜" pins with every third row entirely empty.	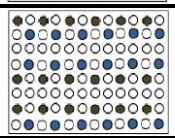
Staggered, Every 3rd Row Empty, ½"	Each row contains half the number of pins alternating pin-hole, next row hole is offset. Every third row entirely empty. ½" pins.	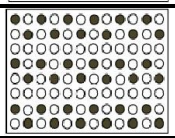

VITA

Carolyn Leigh Thiemann was born on February 22, 1989 in Syracuse, New York. In 2007 Carolyn enrolled at Onondaga Community College where she received her Associates of Science degree in the Engineering Science program before transferring to Syracuse University. There she entered the Aerospace Engineering program and graduated in 2011 with her Bachelor of Science degree. To further continue her education, Carolyn enrolled at the University of Tennessee Space Institute where she is currently being awarded a Master of Science degree in Aerospace Engineering.